THE STRUCTURAL DIVERSITY OF METAL BINDING SITES IN BACTERIAL METALLOPROTEINS: THE DISORDERED IRON-BINDING COIL OF IRON-SULFUR CLUSTER PROTEIN A AND THE STABLE ZINC RIBBON MOTIF OF THE CARBOXYLTRANSFERASE SUBUNIT OF ACETYL-COA CARBOXYLASE

By

Patrick Wallace Bilder

Dissertation

Submitted to the Faculty of the

Graduate School of Vanderbilt University

in partial fulfillment of the requirements

for the degree of

DOCTOR OF PHILOSOPHY

in

Biochemistry

December, 2005

Nashville, Tennessee

Approved:

Richard N. Armstrong

Marcia Newcomer

David E. Ong

F. Peter Guenerich

Gerald J. Stubb

DEDICATION

I would like to dedicate this research to my parents,

Martin and Glenda Bilder

ACKNOWLEDGEMENTS

I wish to express thanks to my PI Dr. Marcia Newcomer, Dr. Svetlana Pakhomova and the rest of the committee (Drs. Armstrong, Guengerich, Stubbs, and Ong) for their tremendous overall contribution to my training. The Vanderbilt Biochemistry Department and the Vanderbilt Interdisciplinary Graduate Program in the Biological Sciences also made a significant contribution in this regard.

Additional thanks is bestowed upon collaborators for 1) the IscA project (Dr. Huangen Ding, Louisiana State University, Department of Biological Sciences) and 2) the carboxyltransferase project (Sandra Lightle, Jeffrey Ohren, and Dr. Graeme Bainbridge from Pfizer Global Research and Development, Ann Arbor, MI and Dr. Grover Waldrop, Louisiana State University, Department of Biological Sciences).

I would also like to acknowledge Dr. Hansen "Tee" Bordelon and Dr. Michael Oldham for providing many useful insights and an enjoyable work environment.

TABLE OF CONTENTS

LIST OF TABLES

LIST OF FIGURES

LIST OF ABBREVIATIONS

RCC, reductive citrate cycle

PFOR- pyruvate:ferredoxin oxidoreductase

KGOR-2-ketoglutarate:ferredoxin oxidoreductase

Fe-S iron-sulfur

IscA/U/S, iron-sulfur cluster protein A/U/S

Fdx, ferredoxin

DTT, dithiothreitol

$HgCl_2$ mercury (II) chloride

PSM, pseudo-symmetric motif

CODH/ACS, carbon monoxide dehydrogenase/acetyl-CoA synthase

HiPIP, high-potential iron protein

CAC,cytosolic aconitase

IRP1,iron regulatory protein-1

ACC, acetyl-CoA carboxylase

BCCP, biotinoyl carboxyl carrier protein

BC, biotin carboxylase; CT, carboxyltransferase

PCC, propionyl-CoA carboxylase

ACP, acyl carrier protein

Ps 12S, *Propionibacterium shermanii* 12S transcarboxylase;

Sa CT, *Staphylococcus aureus* carboxyltransferase

Ec CT, *Escherichia coli* carboxyltransferase

FAS II, bacterial type II fatty acid biosynthesis

KAS, ketoacyl-ACPsynthase

MMCoA, methyl-malonyl CoA

BiSA, bi-substrate analog

NEM, N-ethylmaleimide

HS, Helical Subdomain

MDR, multi-drug resistant

PART A

IRON-SULFUR CLUSTER PROTEIN A

CHAPTER I

INTRODUCTION

Ancient Origins of the Iron-Sulfur Clusters: Iron-Sulfur Chemistry of the First Biochemical Reactions

Consistent with the diverse phylogeny and essential presence of Fe-S proteins in central metabolic pathways, the inorganic constituents of cellular Fe-S clusters are likely to have possessed a fundamental role in the initiation and maintenance of the first biochemical reactions on earth (Wachtershauser 1992; Russell and Hall 1997). A growing body of evidence suggests that the formation of FeS_2 (pyrite) from H_2S (hydrogen sulfide) and FeS (iron sulfide), which is empirically reproducible under extant geological conditions that simulate a primordial geochemical environment (e.g. 100ºC, anaerobic, in a slightly acidic to neutral pH) represented in the earliest sediments and hydrothermal vents, provides the redox energy source that initiated and supported surface-localized autocatalytic, chemoautotrophic biochemical pathways prior to the emergence of an oxygen-driven cellular metabolism (Cody 2004). The standard free energy gain from pyrite formation is shown in the following equation:

$$FeS + H_2S \rightarrow FeS_2 + H_2 \quad \triangle G^{o} = -38kJ/mol$$

Under similar in vitro reaction conditions, the reductive, anabolic capacity of this "FeS/H_2S" energy-coupling system, which in some instances employed additional geochemically-relevant transition metal sulfide catalysts such as NiS, has been demonstrated through the synthesis of alkane thiols, acetate, and pyruvate from CO/CO_2

as well as short peptides from amino acid precursors (Nakajima, Yabushita and Tabushi 1975; Heinen and Lauwers 1996; Huber and Wachtershauser 1997; Huber and Wachtershauser 1998; Cody, Boctor, Filley, Hazen, Scott, Sharma and Yoder 2000; Huber, Eisenreich, Hecht and Wachtershauser 2003). Diverse reactions are catalyzed by Fe,Ni-S/H_2S in these systems, including acid-base assisted addition, substitution, and elimination of thiol/hydroxyl groups, hydride transfer, reductive carboxylation, and carbonyl insertion. The developing transition metal sulfide reaction surface was also equipped to serve as a positively charged anchor for the selective attachment of anionic functional groups at acidic pH, including carboxylates, phosphates, and thiols (Wachtershauser 1988). Validation of the significance of the synthetic chemistry results for understanding biochemical evolutionary mechanisms is provided by analogous reactions in the reductive citrate cycle (RCC), an ancient, autocatalytic carbon fixation pathway. The RCC is utilized in phylogenetically diverse archaebacterial and eubacterial species, many of which are anaerobic/microaerophilic, chemoautotrophic, hyperthermophilic, and localize to deep sea, volcanic vent environments (e.g. of the orders Thermoproteales and Aquificales) (Beh, Strauss, Huber, Stetter and Fuchs 1993). A primordial, geochemically-feasible RCC based on Fe,Ni-S/H_2S chemistry has been retrodicted from the extant RCC (Fig. 1), a pathway that provides the α-keto acid precursors for amino acid, sugar and pyrimidine biosynthesis, acetyl-coA for lipid biosynthesis, and succinate for the production of hemes and chlorophylls (Wachtershauser 1990). Critical biosythetic reactions associated with the exergonic pyrite formation reaction of Fe,Ni-S/H_2S in the proposed, primordial RCC are assumed in the extant RCC by Fe-S cluster enzymes α-ketoglutarate:ferredoxin oxidoreductase (KGOR)

and pyruvate:ferredoxin oxidoreductase (PFOR) (Hugler, Wirsen, Fuchs, Taylor and Sievert 2005).

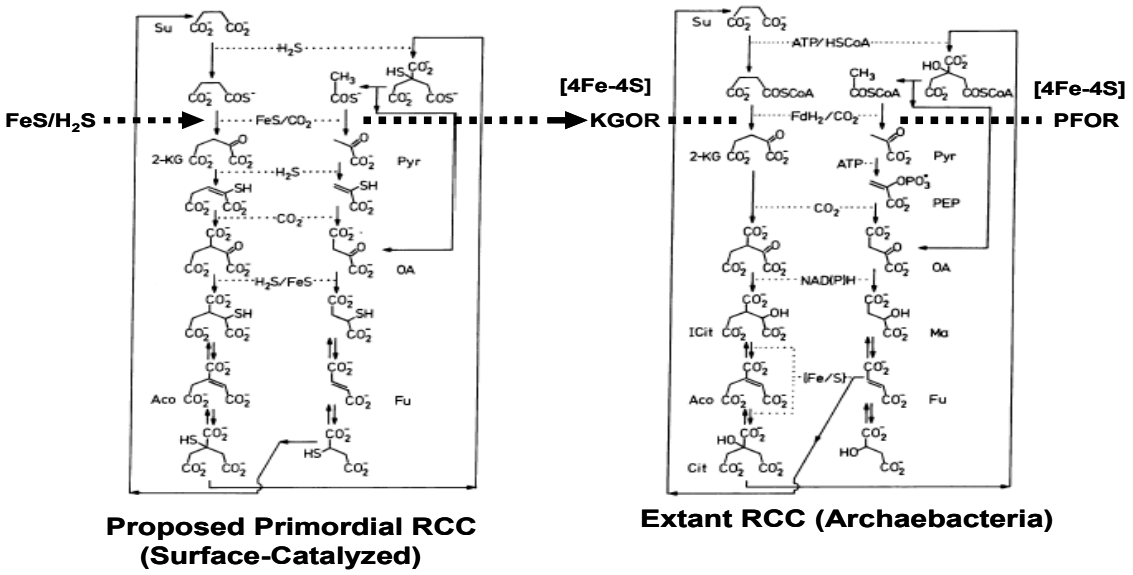

Fig.1 The earliest metabolic pathways were iron-sulfur based. The retrodicted (left) and extant (right) Reductive Citrate Cycle (RCC) pathway (adapted from Wachtershauser 1990)

PFOR and KGOR both require 4Fe-4S ferredoxins, members of the earliest known protein class, to perform 2 electron reductions of succinyl-CoA and acetyl-CoA in the synthesis of the central α-keto acids pyruvate and α-ketoglutarate (Kerscher and Oesterhelt 1981).

An Early Role for Iron-Sulfur Clusters in Energy Metabolism; Iron-Sulfur Cluster Incorporation Into the First Protein Scaffolds

In addition to pyrite, mineral films of diverse FeS-containing nanocrystals of mackinawite ($Fe(Ni,Co)_{1+x}S$), greigite (Fe_3S_4]), and violarite ($FeNi_2S_4$) were likely to

have formed at the interface between hydrothermal, HS- seepage sites in the earth's crust and the acidic, Fe^{2+} rich Hadean ocean (Russell and Hall 1997; Martin and Russell 2003). By analogy to the function of the inner mitochondrial membrane, sieve-like caverns observed in the EM structure of the mackinawite phase were proposed to act as a semipermeable barrier that supported the establishment of an metabolic energy source in the form of an electrochemical gradient at the interface between the acidic, oxidized Hadean seawater and the reduced, basic hydrothermal vent exit sites (Martin and Russell 2003). Electrons derived from H_2 on the vent side are believed to have traversed Fe^{2+} centers in the FeS membrane to a photolytically-generated Fe^{3+} acceptor or a CO_2 acceptor on the ocean side. The presence of polyferrodoxins in thermophilic, anaerobic archaebacteria that reduce CO_2 to methane through H2 oxidation (the methanogens) suggests that these 6 x [4Fe-4S] polypeptides may have ultimately assumed the electron transport function of the mackinawite membrane (Russell and Hall 1997; Johnson, Dean, Smith and Johnson 2005). In addition, many components of the respiratory and photosynthetic electron transport machinery (including ferredoxins), which arose ultimately from bacterial endosymbionts, require multiple [4Fe-4S] cofactors at variable redox potentials. The 4Fe-4S “thiocubane” cluster of proto-ferredoxin is a slightly distorted version of the “cubane” structure of the Fe4S4 subunit in the greigite lattice (Fig. 2) and possesses an redox potential near the H_2 potential (~-450 mV) and between mackinawite (~-380 mV) and greigite (~-500mV) at pH7 (Russell and Hall 1997; Milner-White and Russell 2005). Amino acid composition and sequence analysis of low-potential, prokaryotic ferredoxins reveals that these proteins evolved at a pre-cellularization stage well before the completion of the triplet code and enables the

reconstruction of a symmetrical, homodimeric, 23 amino acid proto-ferredoxin capable of binding a positively charged transition metal sulfide surface through an acidic amino terminal tail (Eck and Dayhoff 1966; Davis 2002). Tandem duplication of the coding sequence of the proto-ferredoxin monomer, which contributes 3 invariant cysteines and swaps a 4th invariant cysteine between two identical consensus 4Fe-4S cluster binding sites in its dimeric form, generates all but 9 residues of the neutrally-charged, extant bacterial form in a single polypeptide (Davis 2002).

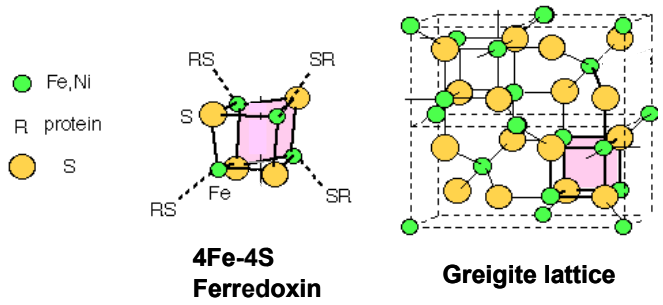

Fig. 2 Similarity of 4Fe-4S ferredoxin to the FeS mineral greigite, a structural component of hydrothermal vents (adapted from Russell et. al 2001)

One common and striking feature of FeS cluster binding proteins such as the ferredoxins is the high proportion of repetetive sequences of glycine and alanine, the earliest encoded amino acids, in loops that provide the cysteinyl iron ligands (Milner-White and Russell 2005). The backbone conformation of these cluster-binding loop motifs, known as “nests”, is arranged such that the amide nitrogens form a positively charged cavity for the insertion of an anionic ligand (Watson and Milner-White 2002; Milner-White, Nissink, Allen and Duddy 2004). Since organic thiolate ligands were likely to have been major constituents of the vent seepage waters, they would have

organized around 4Fe-4S or 2Fe-2S units in the greigite lattice to produce $([Fe4S4]RS4)^{2-}$ clusters, a species which is readily assembled in vitro (Beinert, Holm and Munck 1997; Milner-White and Russell 2005). Prior to the incorporation of cysteine into the coding sequence of surface-localized FeS proteins, short peptides with nest geometries would suffice to stabilize the overall negative charge of clusters derived from the transition metal sulfide catalyst beds. Violarite, generated through the replacement of an Fe center in greigite with Ni, resembles the Fe-Ni-S-containing "A" and "C" clusters of carbon monoxide dehydrogenase/acetyl-CoA synthtase (CODH/ACS), a bifunctional enzyme that drives the anaerobic, reductive acetyl-coA (RAC) pathway through the reduction of CO_2 to CO using 2 electrons supplied by the hydrogens from water, condensation of Ni-bound CO and Ni-bound CH3, and acetyl tranfer to CoA (Rees 2002; Martin and Russell 2003). Although the RAC is linear (ie. not autocatalytic like the RCC), it's highly exergonic nature, widespread presence in archae/bacteria, and the empirical support gained through the success of Fe,Ni-S-mediated catalysis of carbonyl insertion reactions argues that this pathway may also have spawned a broad range of pre-cellular biosynthetic precursors (Cody 2004). The reaction catalyzed by CODH is analagous to the proposed mechanism of electron flow between H_2 and CO_2 across the semipermeable membrane of mackinawite which, upon oxidation, produces the greigite structure (Martin and Russell 2003).

General Biochemical Properties of Protein-Bound Iron-Sulfur Clusters; Protein Structure-Cluster Interactions

The ranging physicochemical properties of iron-sulfur clusters, which are subject to fine tuning in their respective protein binding sites, underlie the chemical elasticity attributed to these cofactors (Beinert, Holm and Munck 1997). All of the major protein-bound iron-sulfur cluster types (Fig. 3), including mononuclear FeS_4 (e.g. rubredoxin), dinuclear 2Fe-2S (e.g. adrenodoxin, Fe hydrogenases), trinuclear 3Fe-4S (e.g. aconitase, Ni-Fe hydrogenase), and tetranuclear 4Fe-4S (associated with numerous ferredoxins, hydrogenases, oxidoreductases), can be easily synthesized at room temperature and interconverted amongst these stable geometries by varying the stoichiometry of Fe^{2+} salts, organic thiols, organic disulfide reductants, and elemental sulfur or sulfide anion (Beinert, Holm and Munck 1997).

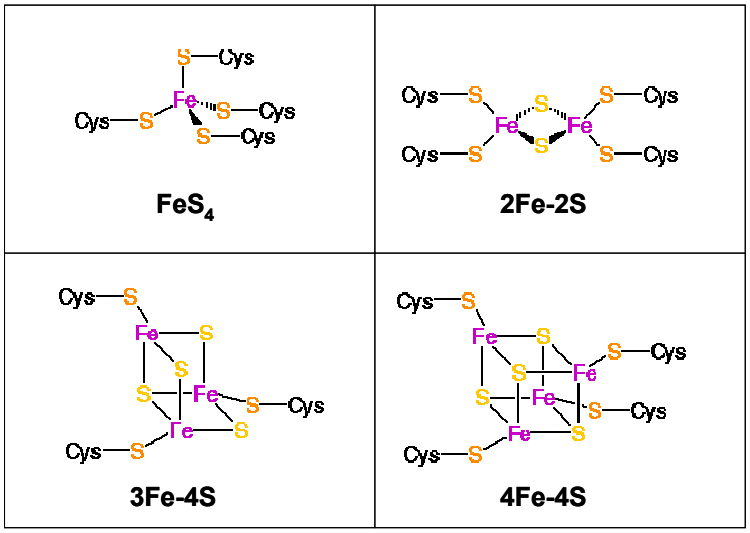

Fig. 3 The major protein-bound iron-sulfur cluster types

Since these reactions proceed in the absence of protein, as they were predicted to have done on primordial transition metal sulfide surfaces, protein scaffolds for iron-sulfur clusters are regarded as cofactor modulators with respect to redox potential and geometry. Depending on the local protein-cluster environment, multiple oxidation states are accessible to each cluster type formed, the number of potential oxidation states increases with nuclearity and a broad range of redox potentials (between -700 mV and +400 mV) are observed over the full set of known biological iron-sulfur clusters (which include low potential ferredoxins containing two 4Fe-4S clusters or 1 4Fe-4S and 1 3Fe-4S cluster as well as high-potential iron proteins, or HiPIPs) (Fig. 4) (Beinert 2000). An examination of the effects of hydrogen bonding, solvent accessibility, charge, and conformational flexibility imposed by the protein milieu on the redox potential of the cluster has been modeled (within an error of ± 50 mV for predicted potentials) using a combined electrostatics/molecular dynamics approach (Protein Dipoles Langevin Dipoles, or PLPD) on a subset of high resolution iron-sulfur cluster protein structures containing representatives from each of the major cluster types (Stephens, Jollie and Warshel 1996).

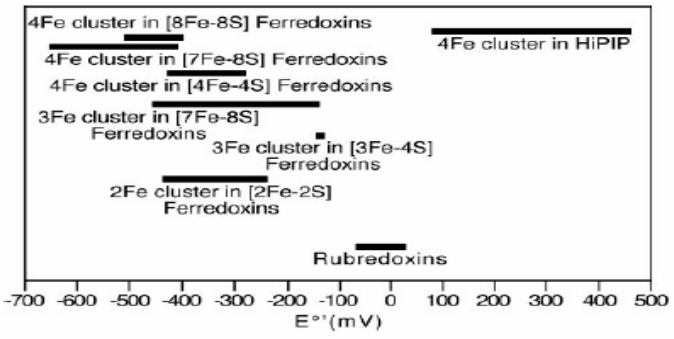

Fig. 4. Variability in the redox potential of protein-bound FeS clusters (Figure from Beinert et al. 2000)

The results suggest that the major determinant of cluster potential (resulting primarily from electrostatic interactions with amide groups) is the backbone configuration surrounding the cluster. Nearby side chains appear to be critical for the protein-cluster interaction only inasmuch as they guide the local main chain conformation or fold. The malleable geometry of iron-sulfur clusters, as exemplified by the iron-sensing 4Fe-4S center of cytosolic aconitase (CAC)/iron regulatory protein-1(IRP1), is often observed in the context of physiological regulation in response to oxidative stress or changes in intracellular iron concentrations (Cairo, Recalcati, Pietrangelo and Minotti 2002). Under conditions that provide a sufficient concentration of cytosolic iron, a distorted, oxidized cubane $[4Fe\text{-}4S]^{2+}$ center exists in substrate-bound CAC: three irons are ligated to cysteines and the fourth iron is coordinated to two isocitrate oxygens and a water molecule (Lauble, Kennedy, Beinert and Stout 1992). Intracellular iron deficiency inactivates CAC enzymatic activity through release of the catalytic iron and formation of a reduced cuboidal $[3Fe\text{-}4S]^{1+}$ cluster (Kent, Dreyer, Kennedy, Huynh, Emptage, Beinert and Munck 1982; Moura, Moura, Kent, Lipscomb, Huynh, LeGall, Xavier and Munck 1982; Kent, Emptage, Merkle, Kennedy, Beinert and Munck 1985). Cluster release effectively shifts CAC into IRP1, a mRNA-binding factor that inhibits ferritin translation and stabilizes transferrin mRNA in a process that restores iron homeostasis by enhancing iron uptake and reducing iron storage, respectively (Zheng, Kennedy, Blondin, Beinert and Zalkin 1992; Beinert and Kiley 1996). Rearrangements in cluster geometry are also observed upon conversion of the cubane 4Fe-4S cluster into the 2Fe-2S rhomb in FNR (fumarate nitrate reductase regulator), an *Escherichia coli* transcription factor that coordinates a global changeover from anaerobic to aerobic metabolism upon exposure to

molecular oxygen (Khoroshilova, Popescu, Munck, Beinert and Kiley 1997). In both the case of both CAC/IRP1 and FNR, the associated cluster reorganizations occur in response to small changes in the concentration of the metabolic regulator and demonstrate full reversibility within minutes, a desirable property for an effective molecular switch. It often appears that the clusters themselves are also capable of driving significant structural rearrangements in the protein(s) to which they are bound. For example, cysteine ligand swapping during cluster transformation has also been observed for the aconitase 3Fe-4S center (Plank, Kennedy, Beinert and Howard 1989). In this instance, a pH-driven conformational change delivers two cysteines from a distant helix to a linear 3Fe-4S cluster in exchange for a cysteinyl ligand coordinated to the original, cubane 3Fe-4S site.

Biological Iron-Sulfur Cluster Assembly

Although the physicochemical constitution of biological Fe-S clusters has been extensively characterized through synthesis of model structures, spectroscopy, and x-ray crystallography, the mechanisms underlying their biosynthesis are currently in an early phase of exploration. Recent genetic studies have demonstrated an essential nature for gene products both within the bacterial iron-sulfur cluster (isc) operon and a corresponding set of predominantly-mitochondrial eukaryotic homologues (Strain, Lorenz, Bode, Garland, Smolen, Ta, Vickery and Culotta 1998; Schilke, Voisine, Beinert and Craig 1999; Lange, Kaut, Kispal and Lill 2000; Schwartz, Djaman, Imlay and Kiley 2000; Tokumoto and Takahashi 2001). Complementary biochemical analyses of these proteins suggest that they function to coordinate binding and assembly of Fe-S clusters

which are ultimately transferred to critical Fe-S containing target proteins (Agar, Krebs, Frazzon, Huynh, Dean and Johnson 2000; Kato, Mihara, Kurihara, Takahashi, Tokumoto, Yoshimura and Esaki 2002; Mansy, Wu, Surerus and Cowan 2002; Muhlenhoff, Richhardt, Gerber and Lill 2002; Tokumoto, Nomura, Minami, Mihara, Kato, Kurihara, Esaki, Kanazawa, Matsubara and Takahashi 2002; Wu, Wu, Surerus and Cowan 2002; Yoon and Cowan 2003). Disruption of both isc genes and their eukaryotic orthologues substantially reduces the activity of the Fe-S cluster containing enzymes and oxygen/iron sensor proteins with central roles in the regulation of the citric acid cycle or the electron transport machinery (Strain, Lorenz, Bode, Garland, Smolen, Ta, Vickery and Culotta 1998; Schilke, Voisine, Beinert and Craig 1999; Schwartz, Djaman, Imlay and Kiley 2000; Tokumoto and Takahashi 2001). In current models (Fig. 5), Fe-S cluster biosynthesis in the bacterial cytosol is initiated by IscS, a cysteine desulfurase which generates sulfane sulfur on the surface of IscU or IscA, homodimeric scaffold proteins which mediate sequential assembly of transiently-bound [2Fe-2S] and [4Fe-4S] clusters (Agar, Zheng, Cash, Dean and Johnson 2000; Agar, Krebs, Frazzon, Huynh, Dean and Johnson 2000; Krebs, Agar, Smith, Frazzon, Dean, Huynh and Johnson 2001; Kato, Mihara, Kurihara, Takahashi, Tokumoto, Yoshimura and Esaki 2002; Wollenberg, Berndt, Bill, Schwenn and Seidler 2003). Holo-IscA and eukaryotic homologues of IscA/IscU (IsA/IsU) have been shown to complex and transfer [2Fe-2S] clusters to the apo-form of a conserved [2Fe-2S] ferredoxin (Fdx in *E. coli*), also synthesized from the isc operon (Ollagnier-de-Choudens, Mattioli, Takahashi and Fontecave 2001; Wu, Mansy, Wu Sp, Surerus, Foster and Cowan 2002; Wu, Wu, Surerus and Cowan 2002; Wollenberg, Berndt, Bill, Schwenn and Seidler 2003). IscA/IsA may also serve as a

direct iron donor for the iron-sulfur cluster assembly process, as discussed in further detail later. Fdx appears to play a role similar to its yeast homologue, Yah1p, an essential mitochondrial ferredoxin which is required for the assembly of Fe-S prosthetic groups in both intra- and extra-mitochontrial enzymes (Takahashi and Nakamura 1999; Lange, Kaut, Kispal and Lill 2000). A recent NMR study of bacterial (*Thermotoga maratima*) IscU describes a unique metallochaperone structure which, as a result of inherent conformational flexibility, lacks stable tertiary structure in both the unbound and Fe-S cluster-bound states (Bertini, Cowan, Del Bianco, Luchinat and Mansy 2003). Deuterium exchange measurements coupled with ^{1}H-^{15}N HSQC spectra positioned two of three conserved cysteine ligands (C38,C63) in a proximal arrangement within the Fe-S cluster binding pocket, an area of defined, albeit dynamic, loop regions immediately flanking ordered secondary structural elements.

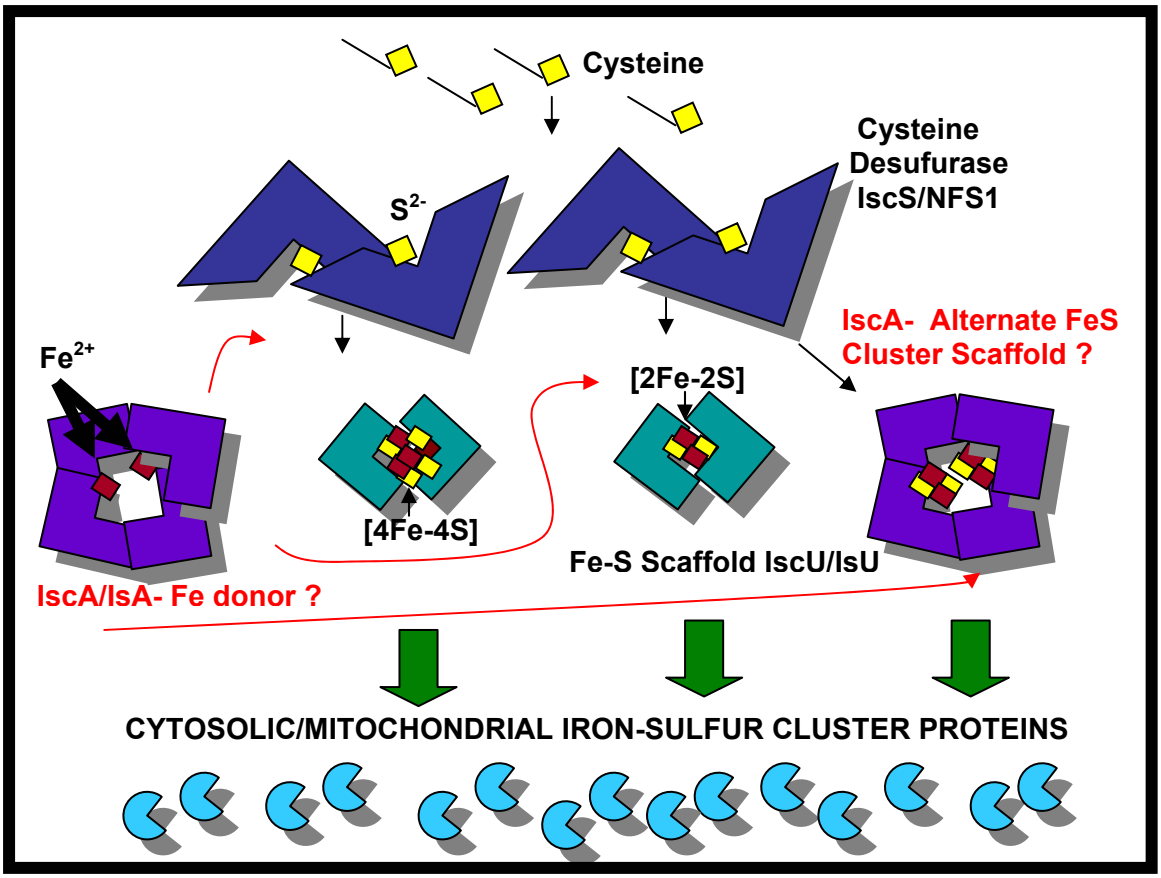

Fig. 5 A current model for iron-sulfur cluster assembly (in the bacterial cytosol and eukaryotic mitochondrion). Members of the *E. coli* isc operon are listed first, followed by their mitochondrial counterparts.

Iron-Sulfur Cluster Scaffold Proteins and the Role of Iron-Sulfur Cluster Protein A

Although in vitro kinetic and steady state spectroscopic data suggest that IscU/IsU and IscA/IsA assemble solvent-accessible, labile Fe-S clusters and transfer these clusters to apo-ferredoxin at similar rates, there are noteworthy differences which imply that these proteins are not functionally redundant. IscA/IsA and IscU/IsU, although highly conserved, lack sequence homology. IsA binds Fe-S clusters with a higher affinity than IsU, and IsA recognizes a binding site on the target ferredoxin distinct from IsU (Krebs, Agar, Smith, Frazzon, Dean, Huynh and Johnson 2001; Wu, Wu, Surerus and Cowan

2002; Wollenberg, Berndt, Bill, Schwenn and Seidler 2003; Wu and Cowan 2003). Interestingly, IscA but not IscU can be overexpressed and purified with an accompanying, high affinity binding site for mononuclear iron with tetrahedral ligation (Ding and Clark 2004). Since incubation of iron-loaded IscA with apo-IscU, cysteine and IscS was sufficient for the assembly of a [2Fe-2S] cluster on IscU, this data suggests that IscA may constitute the as-yet unidentified iron donor for the Fe-S cluster assembly process. The requirement for such an iron-binding protein results from the need to simultaneously maintain free cellular iron concentration at low, non-toxic levels and to achieve high effective concentrations of Fe for Fe-S cluster assembly and incorporation into essential enzymes with Fe-S prosthetic groups. This hypothesis is supported by the observation that deletion of the gene encoding the yeast mitochondrial IscA homologue, Isa1p, which bears 50% similarity to IscA, produced high levels of mitochondrial iron and corresponding oxidative damage to the mitochondrial genome in addition to complete inactivation of the Fe-S enzymes acitonase and succinate dehydrogenase (Jensen and Culotta 2000). Likewise, removal of Isa1p from mitochondrial extracts supplied in an radioassay which fully reconstitutes the Fe-S protein maturation pathway markedly inhibited [55-Fe] incorporation into an internal biotin synthase standard (Muhlenhoff, Richhardt, Gerber and Lill 2002). Mutagenesis in Isa1p of any of the three invariant cysteine residues (present in IscA/IsA proteins as C1-X(n)-C2-X(1)-C3) produced similar mitochondrial defects and inhibited growth on non-fermentable carbon sources, suggesting a function for these residues in both both mononuclear iron and Fe-S cluster ligation (Kaut, Lange, Diekert, Kispal and Lill 2000). Mutagenesis of C2 and C3 to serine in *E. coli* IscA (C99S and C101S, respectively) abolishes the iron center and

addition of cysteine to the wild type protein releases ferrous iron into solution (Ding, Clark and Ding 2004). As the iron:monomer ratio was demonstrated to be 2:1 in the iron-saturated protein, *E. coli* IscA appears to contribute C99 and C101 as ligands for an iron atom situated between monomers. In addition, two of the three invariant cysteines (C2,C3) in a cyanobacterial IscA (the *Synechocystis* PCC 6803 slr1417 gene product), a protein that purifies from this organism as an iron-bound species, were shown to be essential for the coordination of a [2Fe-2S] cluster whereas alanine substitution of C1 weakened cluster formation by 40% (Wollenberg, Berndt, Bill, Schwenn and Seidler 2003). The absorption and Mossbauer spectra which supported these findings were consistent with tetrahedral thiolate ligation of one [2Fe-2S] cluster per dimer by C2 and C3, or one Fe-S cluster bound between monomers (Wollenberg, Berndt, Bill, Schwenn and Seidler 2003). Similarly, serine substitution of C1,C2, or C3 in IsA significantly weakened, but did not abrogate, [2Fe-2S] cluster binding and accelerated cluster transfer to apo-ferredoxin (Wu and Cowan 2003). In contrast to cyanobacterial IscA, Mossbauer spectroscopic data left open the possibility that one or more oxygen or nitrogen ligands were coordinated to the [2Fe-2S] cluster of IsA (Wu, Mansy, Hemann, Hille, Surerus and Cowan 2002).

Purpose

Although significant progress has been made towards understanding the mechanisms of biological iron sulfur cluster assembly by members of the isc operon, a detailed understanding of its structural basis is only beginning to emerge. Despite the availability of high resolution x-ray structures of several *E. coli* isc proteins, including

cysteine desulfurase and the [2Fe-2S] ferredoxin, at the time this study was conceived there was no structural information pertaining to either of the key iron-sulfur cluster scaffold proteins, IscU or IscA. Since preliminary results since published (Ding and Clark 2004; Ding, Clark, and Ding 2004) suggested that IscA was potentially bifunctional (ie. as an iron donor for iron-sulfur cluster assembly and/or an alternative scaffold to IscU for iron-sulfur cluster transfer), essential and fundamental to the biological cluster assembly process, the prospect of an X-ray structure for IscA was both intriguing and promised to lend new insights into the mechanism of iron-sulfur cluster assembly.

CHAPTER II

MATERIALS AND METHODS

Crystallization and Data Collection

E. coli IscA was over-expressed from a C-terminal, 6-His-tagged construct and purified to homogeneity as described by Ding and coworkers (Ding and Clark 2004). IscA was subsequently desalted using a PD10 column, concentrated to 17 mg/ml, and incubated at 4 ºC overnight with 1.1 mM ferrous ammonium sulfate and 2 mM DTT. Under a glove bag enclosing a helium atmosphere, crystals were grown at room temperature by the vapor diffusion method in drops containing 0.8-1.0 M dibasic ammonium phosphate buffered with 0.1 M imidazole, pH 8.0. Hexagonal, rod-shaped crystals (Fig. 6) of the dimensions ~0.2 x 0.2 x 0.7 mm appeared in the presence of 10 mM Mercury (II) chloride ($HgCl_2$) supplemented in the mother liquor (derivative conditions) or its absence (native conditions) and grew to near maximal size within 2-4 weeks. IscA crystals belong to the space group $P6_2$ with unit cell lengths a=55.5, c=159.0 Å. The estimated solvent content is 55% with a dimer in the asymmetric unit.

Fig. 6 Representative native IscA crystals

Diffraction data for a single native and derivative crystal (Fig. 7) were collected at 100K on a Mar345 image plate detector mounted on a Nonius FR591 rotating CuKα anode fitted with Osmic mirrors. Crystals were transferred to a cryoprotectant solution containing 20% ethylene glycol/80% mother liquor immediately prior to freezing. The

crystal-to-detector distance was 160mm for 1º oscillation images, each exposed for 30 minutes.

Table 1

Diffraction Data Statistics[a]						
dataset	**resolution (Å)**	**completeness (%)**	**total/unique reflections**	**I/σ**	**redundancy**	**Rsym[b] (%)**
Native	**∞-2.65**	**99.8(100.0)**	**77,724/8,034**	**58(5.5)**	**9.7(9.9)**	**6.6(47.9)**
$HgCl_2$	**∞-2.30**	**99.4 (99.1)**	**67,990/12,243**	**38(3.7)**	**5.6(5.3)**	**6.3(45.7)**

Phasing Statistics- SIR									
Deriv	**Sites**	**Occ (sites 1/2/3)**	**Res (Å)**	**P hasing power[c] acentric**	**centric**	**Rcullis[d] acentric**	**centric**	**FOM[e] acentric**	**centric**
$HgCl_2$	**3**	**0.89/0.88/0.11**	**27-2.8**	**1.54**	**1.27**	**0.66**	**0.67**	**0.36**	**0.63**

[a]The values in parentheses are for the highest resolution shell.[b]Rsym=∑(I-<I>)/ ∑(I) where I is the intensity measurement for a given reflection and <I> is the average intensity for multiple measurements of this reflection.[c]Phasing power=heavy atom structure factor/root-mean-square lack of closure error (statistics from CNS).[d]Rcullis=lack of closure error/iso-ano difference (generalized Rcullis in CNS).[e]FOM is the figure of merit.

Each of these datasets were indexed and processed with Denzo, a software package that enables automated integration of observed intensities across diffraction maxima (with associated background) and the precise location of these reflections in reciprocal space (a geometric assignment based on the wavelength of the radiation, the crystal-to-detector distance, and the crystal lattice planes from which the radiation was scattered) (Otwinowski and Minor 1997). Denzo also provides penalties associated with distortion to a lattice type with higher symmetry than triclinic, which lacks symmetry (except for an inversion center). The dataset outputs from Denzo were individually scaled with Scalepack, a program that merges reflections and background from all individual diffraction images (collected by incrementally oscillating the crystal about a fixed axis),

corrects measured intensities and their associated errors for scattering effects related to beam polarization and detector geometry, and places the intensities an absolute scale that additionally depends on a user defined error model and the assigned space group symmetry (Otwinowski and Minor 1997). In addition to reporting the refined unit cell geometry and the mosaicity associated with lattice imperfections, Scalepack tabulates Rsym, the overall goodness of fit between symmetry-related reflections, Redundancy, the average number of times a unique reflection is observed by symmetry, and $\langle I \rangle / \sigma$, the average signal to noise ratio, by resolution shell. It also reports the indices assocated with systematic absences in the diffraction pattern, an indicator of point group symmetry. Both datasets yielded good statistics in terms of Rsym, $\langle I \rangle / \sigma$, and redundancy through 2.65Å and 2.35 Å for the primitive hexagonal lattice assigned to the native and derivative IscA datasets, respectively.

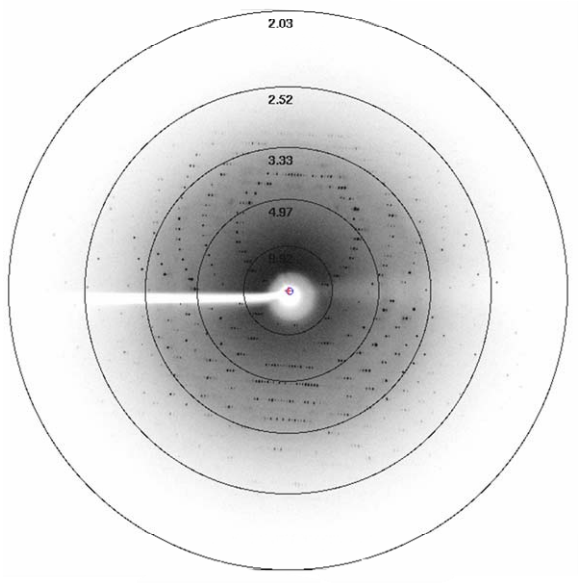

Fig. 7 Representative native IscA diffraction

Table 2

	Native	$HgCl_2$
resolution (Å)	27-2.65	27-2.3
number of reflections	7,371	11,110
sigma cutoff	none	none
R_{factor} (%)	23.2	22.9
R_{free}(%)[a]	25.6	26.3
number of refined atoms:		
protein	1,470	1,470
water	61	85
average B factors (Å^2):		
protein	42.0	43.7
water	40.2	43.6
Hg^{2+}	NA	72.2
Overall	42.0	43.8
B from Wilson plot	56.6	44.2
rms deviations:		
bonds (Å):	0.010	0.014
angles (°):	1.4	1.5
Ramachandran plot		
most favored regions (%)	93.8	94.4
additional allowed (%)	4.9	5.6
disallowed (%)	1.2*	0.0

[a]R_{free} was calculated from 5% of the diffraction data and monitored throughout refinement.
*Corresponds to residue cysteine 35 from both monomers in the asymmetric unit.

The unit cell axes (of the primitive hexagonal lattice) differ only insignificantly (native: a=55.527, c=159.037, derivative: a=55.337, c=159.834) and therefore satisfy the phasing criteria that the unit cell dimensions are isomorphous. Although the point group symmetry was still uncertain at this stage, the list of systematic absences implied that $P6_2$, $P6_4$, and the related space groups $P6_222$and $P6_422$ were likely. Non-hexagonal lattice types were excluded because of their high penalties from the indexing routine. For both datasets, each I and its associated error σI for all indices (the Scalepack output) were converted to observed structure factor amplitudes (Fo=sqrt I) and associated errors (σFo=Fo-sqrt (I-σI) if I>σI or σFo=Fo if I≥σI) in CNS (Brunger, Adams, Clore, DeLano, Gros, Grosse-Kunstleve, Jiang, Kuszewski, Nilges, Pannu, Read, Rice, Simonson and Warren 1998). Final statistics from intensity data processed with Denzo and scaled in

Scalepack are listed in Table 1. The high redundancy and signal to noise ratio of the diffraction data allowed us to include reflections to resolutions of 2.65Å (native) and 2.3Å (derivative) in the final refinements (Table 2).

Structure Determination and Refinement

Co-crystallization of IscA with $HgCl_2$ noticeably enhanced the size, morphology and diffraction quality of the crystals. An overall R_{merge} of 18.0% for native and $HgCl_2$-IscA structure factor amplitudes to 2.7Å was indicative of a heavily substituted derivative. Three heavy atom binding sites in the asymmetric unit, two of which appeared definitively on the Harker sections (Fig. 8) and refined to high occupancy values, were identified through an automated Patterson search in CNS and used to calculate initial SIR phases to 2.8Å (Table 1). An electron density map calculated from solvent-flattened SIR phases (using the program DM in CCP4 (1994), overall Figure of Merit=0.47) revealed, after skeletonization in MAPMAN (Kleywegt and Jones 1996) and visualization in O (Jones, Zou, Cowan and Kjeldgaard 1991), salient secondary structural features (Fig. 9).

One pair of overlapping, albeit disjointed, β sheets was sufficient to elucidate a 2-fold non-crystallographic symmetry (NCS) axis and to generate an initial matrix for the production of an improved, averaged map in DM. This map served as a starting point for the construction of a poly-alanine backbone. After iterative cycles of model building in O, SigmaA weighting, phase combination, solvent flattening and phase extension in CCP4, and rigid body refinement and energy minimization in CNS, a majority of the side chains were identified.

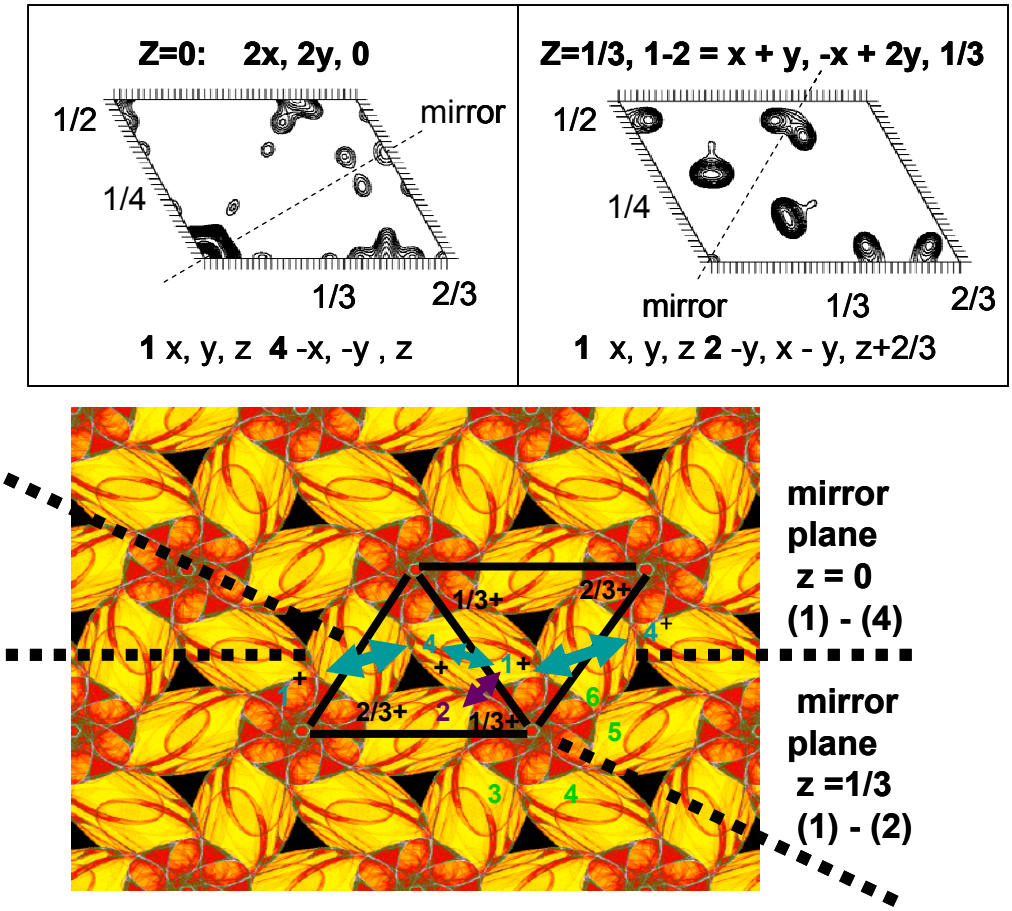

Fig. 8 Harker peaks for $P6_2$ (top) and schematic of corresponding molecular vectors in the unit cell (bottom)

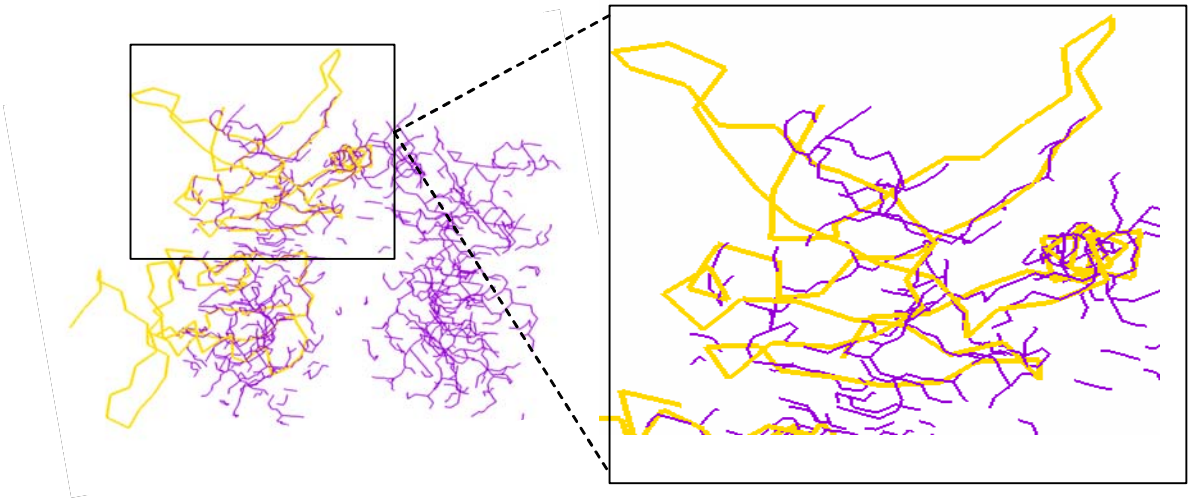

Fig. 9 Mapman bones model. magnification of bones model created in mapman (purple) Highlights starting point for early backbone tracing after density modification. The final Cα trace is in yellow.

In the early stages of refinement and interpretation of 2Fo-Fc maps, the structure factor amplitude array from the higher resolution, derivative dataset was employed. As R factors dropped below 0.30, it became clear that independent monomers were nearly identical, and the model improved as high NCS restraint weights (400 in CNS) were imposed. Further refinement cycles that included energy minimization, B-group refinement, and simulated annealing were conducted using maximum likelihood refinement in CNS. Concluding stages of refinement were carried out in REFMAC5 (CCP4) (Murshudov, Vagin and Dodson 1997). Monomers in the final models lack the last 10 residues present in the native protein, including Cys99 and Cys101. A Ramachandran plot in PROCHECK (Laskowski, MacArthur, Moss and Thornton 1993) demonstrates favorable main chain geometry for both the native and Hg-IscA structures with the exception of a single non-glycine outlier, Cys35, in the native model. In a 2Fo-Fc omit map produced from the derivative dataset, density corresponding to each Cys35 thiol is enveloped in a 17 sigma Hg peak, consistent with covalent binding of the metal at

this position.. The final R/R_{free} for the native and derivatized structures are 23.2/25.6 and 22.9/26.3%.

CHAPTER III

RESULTS AND DISCUSSION

Overall Fold

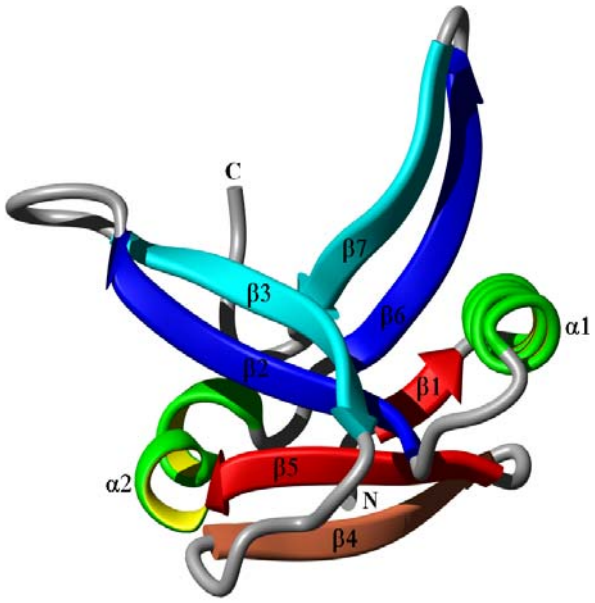

Fig. 10 A ribbon diagram showing the secondary structural elements in the IscA monomer

The absence of proteins in the Dali database that bear significant structural homology to IscA suggests that IscA adopts a novel protein fold. This fold is characterized by a striking, internal two-fold symmetry such that the unique portion of the structure covers roughly 50% of the primary sequence (Fig. 10). A complete IscA monomer includes tandem pseudo-symmetric motifs (PSM) 1 (β1-α1-β2-β3) and 2 (β5-α2-β6-β7) separated by a unique, near-palindromic, 14 amino acid stretch (E_{43}FVDEPTPEDIVFE_{56}) encompassing the 3 C-terminal residues of β3, a short, 6-residue loop region, and 5 of the 6 residues which constitute β4 (Fig. 11). Identifiers for residues related on the virtual two-fold are colored identically (F44/55-violet, E43/56-brown, V45/54-green, D46/52-turquoise, E47/51-brick red, P48/50-blue). T49, at the palindrome center, is black and I53, labeled red and in parentheses, is not shown.

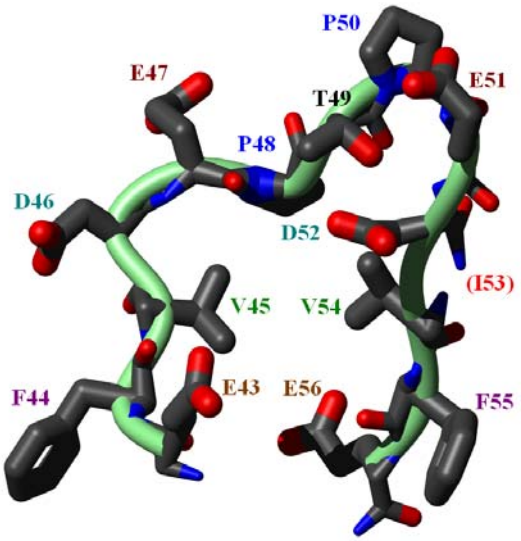

Fig. 11.Structure of the 14-residue pseudo-palindromic amino acid sequence in IscA

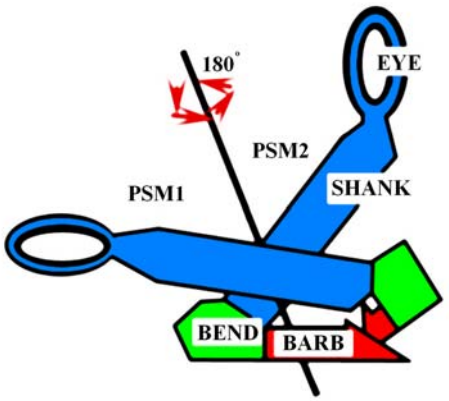

Fig. 12 A schematic representation of the IscA monomer fold as a pair of interlocked fish hooks

PSM1 and PSM2 each resemble a fish hook twisted at the bend so as to create a 45 degree angle between the barb and the shank (Fig. 12). Each hook represents a single pseudo-symmetric motif (PSM). Elements related by pseudo-two-fold symmetry are colored identically (β1,β5 or barbs-red, α1,α2 or bend-green, β2,β6-blue, β3,β7-cyan or shank-light blue). The β-4 strand, which is cut by the pseudo-two fold axis, is depicted in brown in Fig. 11. In PSM 1/2, β1/β5 lies along the barb, α1/α2 traverses the bend, and β2-β3/β6-β7 extend the shank as a twisted, antiparallel β sheet. If the IscA monomer constitutes the fundamental building block of a ladder that represents an oligomeric state (Fig. 13), the hooks are interlocked such that the barb of PSM1 (β1) points inward at a 45° angle, the bend of PSM1 (α1) rests on the style and its shank (β2,β3) stretches the length of the upper rung. The barb of PSM2 (β5) lies atop the shank of PAM1 (β2) from its midpoint to the style, its bend (α2) becomes the lower right helix of a circular cavity,

and its shank (β6,β7) juts downward to fill the distance between joints at an angle perpendicular to the shank of PSM1.

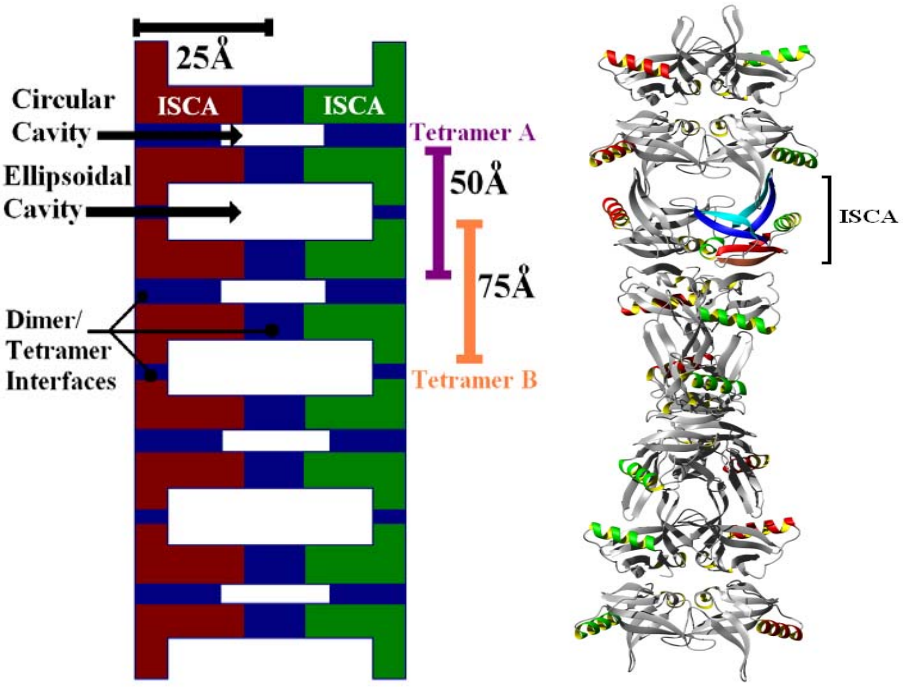

Fig.13 Cartoon representation (left) of the IscA super-helix (right) as a ladder

The resulting architecture is a β sandwich domain composed of two mixed β sheets: a 4-stranded, twisted β4-β5-β2-β3 sheet and a 3-stranded, twisted β1-β6-β7 sheet, offset by 50° to achieve tight, extensive hydrophobic packing at the core.

Examination of the crystal packing of IscA monomers reveals a super-helical assembly with a radius of 25Å and a pitch delimited by three arbitrarily-designated, tetrameric assemblies, each translated 50Å along the helical axis (Fig. 13). Upon this axis, the IscA monomer follows a spiraling, ladder-like pathway stabilized by dimer/tetramer interfaces which occur in regions resembling either joints or the midpoints

of adjacent rungs or interceding styles (i.e. vertical segments between the rungs) of the ladder. Two distinct tetrameric arrangements are possible: one in which four monomers surround a central ellipsoidal cavity ~45Å wide and 7Å tall (for the sake of discussion, tetramer A) and one in which the monomers surround a cylindrical cavity with a 5Å radius (tetramer B). Both orientations are dimers of dimers.

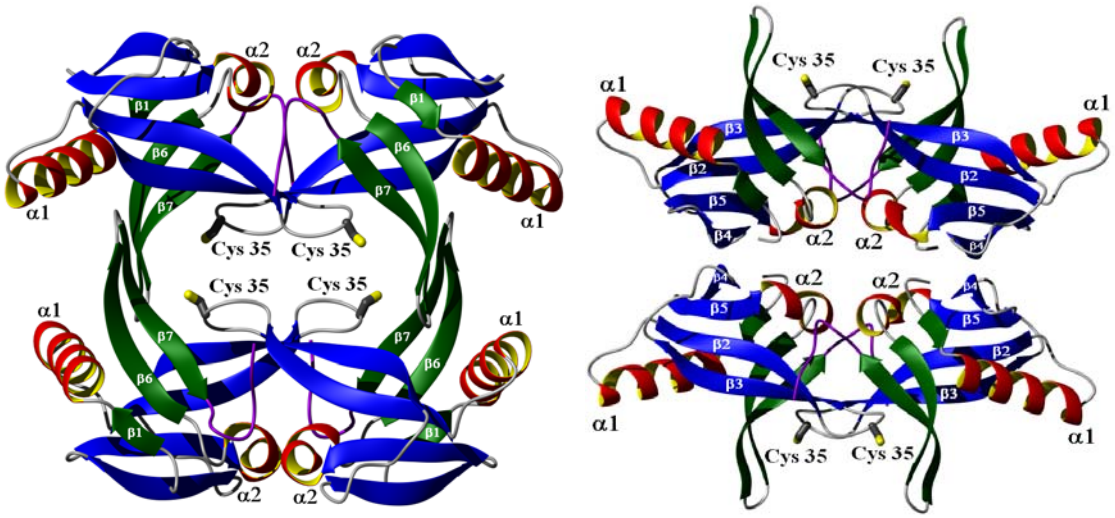

Fig. 14 The possible IscA tetramers. Tetramer A (left) and tetramer B (right)

In tetramer A, the monomers are positioned at the four corners of a picture frame and each contributes the shanks of the fish hooks to its neighbors (Fig. 14). PSM 1 forms a semicircular, 8-stranded β-sheet and PSM 2, a 4-stranded β-sheet with the dimer mates. In tetramer B, 4-stranded β3-β2-β5-β4 sheets of neighboring monomers are joined through β4-β4 and β3-β3 hydrogen bonds to form 90° arcs over a topologically circular palindrome that spirals into a 16-stranded β barrel enclosing the circular cavity (Fig. 14).

Both the purified bacterial protein and its eukaryotic homologues have been

shown to exist in dimeric, tetrameric, or higher order aggregation states (Kaut, Lange, Diekert, Kispal and Lill 2000; Ollagnier-de-Choudens, Mattioli, Takahashi and Fontecave 2001; Wu, Mansy, Hemann, Hille, Surerus and Cowan 2002), and tetramers A or B represent two possible models for the oligomeric states observed in solution. Each of two tetrameric configurations buries ~25% (5600-6100 $Å^2$) of solvent-accessible surface area in dimer/tetramer interfaces between adjacent IscA subunits, suggesting that either tetramer A or tetramer B can exist as a physiologically-stable entity. The unique areas of contact for the independent assemblies (2000 $Å^2$ at the midpoints of styles composing tetramer A or 1500 $Å^2$ at the mid-rung region that joins dimers from tetramer B) are each sufficient for a functional oligomeric interface. The β4-β4 dimerization interface unique to tetramer B is predominantly stabilized by main chain hydrogen bonds from I53, V54, and F55 and van der Waals interactions between I53 side chains on opposing strands. The additional surface area that selectively stabilizes tetramer A is characterized by favorable ionic interactions involving the guanidinium group of R12, which extends from the α-1 helices of one dimer partner to the mid-style E86 carboxylate on β7, an edge on face stacking arrangement of F79 and F88 which restrains the linear conformation of the β6-β7 shanks as they exit the protein core, and the insertion of L84, situated at the eye of the β6-β7 shanks, into a dense hydrophobic pocket of F16, L42, and F44 on the opposite monomer. This constellation of residues, and particularly those that are both hydrophobic and highly conserved or invariant (L42, F44, F79, F88-see Fig. 15), maintains the backbones of the β7 strands at the borders of a channel enclosing six ordered water molecules. Due to the favorable packing at this interface, a feature which relies upon the specific R12-E86 ionic interaction, the conserved hydrophobic network, and the presence

of an extensively hydrogen-bonded water channel, we propose that tetramer A and the dimeric substructure maintaining these contacts represent the most likely oligomeric states in the aqueous *milieu* of the cell.

Conservation in Sequence and Structure

IscA orthologues maintain a high degree of evolutionary conservation as highlighted by a sequence alignment for representative species from each kingdom (Fig. 15).

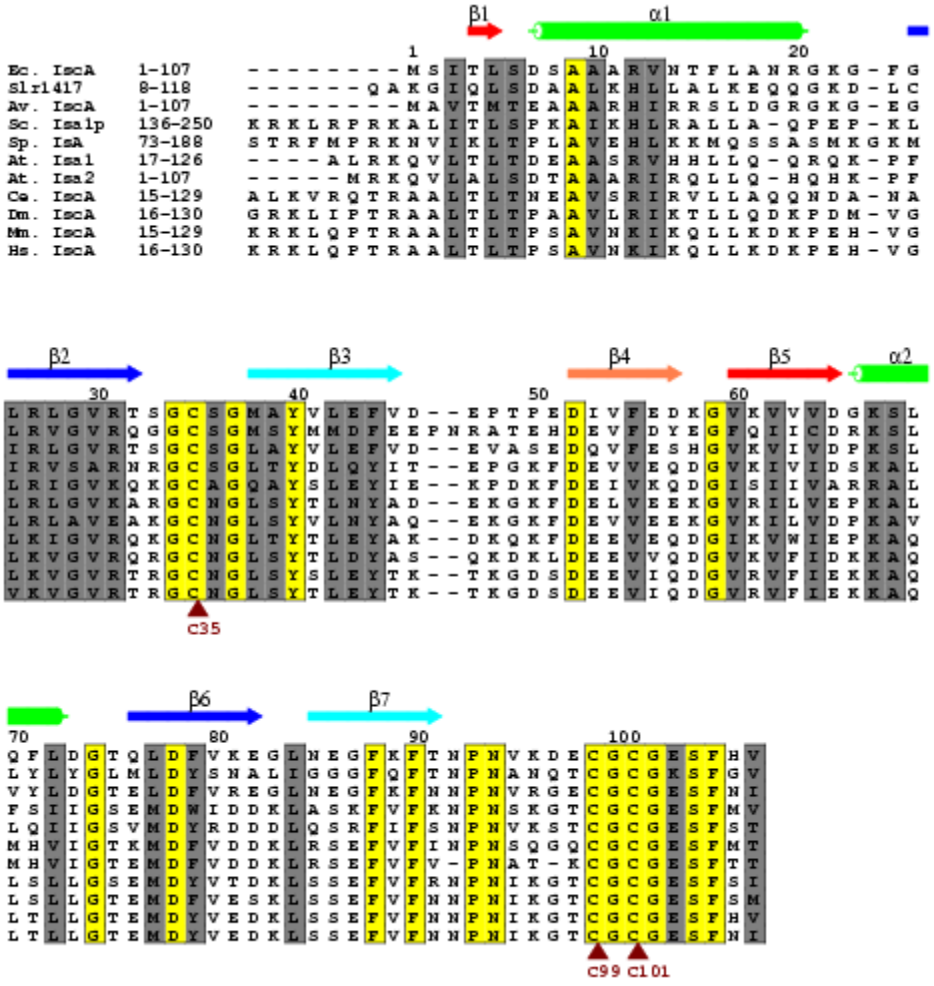

Fig. 15 Sequence alignment of IscA orthologues

In figure 15, residues from IscA/IsA from *E. coli* (Ec), *Synechocystis* PCC 6803 slr1417 (slr1417), *Azotobacter vinelandii* (Av), *Saccharomyces cerevisiae* (Sc), *Saccharomyces pombe* (Sp), *Arabidopsis thaliana* (At), *Caenorhabditis elegans* (Ce), *Drosophila melanogaster* (Dm), *Mus musculus* (Mm), and *Homo sapiens* (Hs) are shown. Amino acids that are conserved in all sequences are highlighted in yellow and highly conserved residues are highlighted in gray. Invariant cysteines 35, 99, and 101 of *E. coli* are marked by brown triangles. Secondary structure elements are indicated above the sequence for *E. coli* IscA and shaded using the same color scheme as in the ribbon model (Fig. 15). Over the 107 amino acid stretch present in the bacterial forms, 47% (50) of residues are highly conserved and 18% (19) are identities. Most of the highly conserved residues (60%) are located within secondary structural elements and a majority of these (67%) contribute to the hydrophobic core that seals the twisted β sandwich domain of IscA. When viewed from a perspective down the intra-molecular two-fold, the hydrophobic side chains fill a rectangular slab bounded by the α-helices on the short edges, the β sheets on the long edges, and the β4 strand at its base. Hydrophobic packing of conserved residues F55,I3,L5,A9/10,V60/62/64,L77,L26,L28,V13,L72,F79,L17,F16,F88,F90,F71,F44,L42, Y40,M38, and V30 occurs progressively upwards in a "knobs in holes" type fashion similar to that described for α-helices. Accompanying side chains stack tightly near the α-β corners or between 3-4 hydrophobic functional groups protruding from two opposite strands above and below the plane of the "knob". Other conserved residues which maintain the integrity of the IscA structure include conserved residues E56(β4) and S6(β1)(consensus S/T), invariant residues D52(β4) and D78(β6), and R27(β2)/K61(β5) (consensus R/K). Intra-molecular salt bridges consisting of D52-R27 and E56-K61 tether

the conformation of the β4-β5-β2-β3 sheet and a D78-S6 hydrogen bonding interaction secures β1-β6 contacts at the turn into the α1 helix. Three invariant glycine residues- G37, G59, and G74- are ostensibly required for transitions into β3, β5, and β6 as they are located in turns immediately before the initiation of these strands. The placement of conserved residues at critical positions in the tertiary structure suggests that the overall fold of IscA has been strictly preserved throughout evolution.

The Cysteine Pocket

Only the first of the three invariant cysteines (C35, C99, C101) implicated in ligation of iron-sulfur cluster complexes is visible in the electron density. C35 is located within two bulging pockets (10Å tall) found on each side of the centrally compressed (7Å tall) ellipsoidal cavity of tetramer A (Fig. 14) On both faces of the cavity, C35 projects from monomers on diagonally opposite corners of the frame (related by the dimer two-fold) into opposite bulges from a flexible, conserved GCXG loop between β6 and β7. At one face, C35 residues are separated by 20Å and located at equivalent positions, each at the eye of a PSM2 shank protruding from the cavity roof and floor. In the native structure the B-factor for the $GC_{35}XG$ region deviates substantially from the mean protein B (+1.6 fold) and C35 is a unique Ramachandran outlier. In contrast, this same region is well ordered in the Hg-derivatized structure (the B-factor is only 1.2 times greater than the mean protein B-factor). Apparently, the covalent binding of Hg to the labile cysteine imparts rigidity to this flexible loop. In addition, the side chain of E82, located on the β6 strand of an adjacent dimer partner, is positioned in the mercury binding pocket of the derivative and rotated 180º away from a solvent-exposed orientation observed in the

native structure. This motion adjusts the side chain carboxyl from 9Å (native) to 4Å and 3.7Å from the C35 thiol and mercury, respectively (Fig. 16). If Hg is instead modeled as an Fe sphere within or near the Hg binding site, it would be positioned to accept an oxygenic ligand from E82 (or the shorter S/D side chains in some IscA homologues). In the native, unligated structure, the Hg-binding pocket of tetramer A likewise contains sufficient volume to accommodate [2Fe-2S] or [4Fe-4S] clusters.

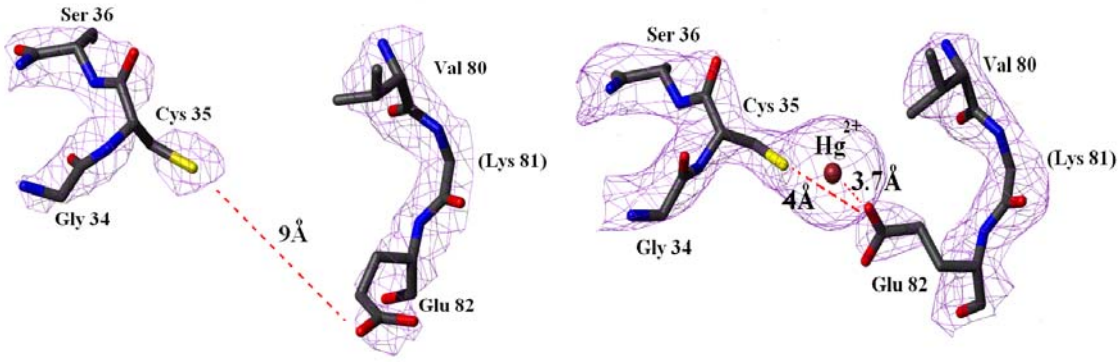

Fig. 16 Conformational adjustments in the C35 pocket induced by Hg binding

Despite the presence of a protein-bound, mononuclear iron center in solution prior to crystallization, electron density for iron is conspicuously absent from the oligomeric, crystalline native state. In addition, a consensus C-terminal stretch CGCGESF containing the other putative iron-binding cysteine residues, C99 and C101, is completely disordered, as judged from the fact that it is not visible in the electron density map. This sequence is located at the end of a coil which begins at the end of β7, turns sharply at an invariant proline (P93) and extends superficially down the center of the upper dimer to the last visible residue, D97, at the brink of the central cavity. Fig. 17 shows electron density (violet) from final, native 2.65Å 2Fo-Fc maps contoured at 1σ in the region

encompassing the last visible C-terminal residues (T91-D97). Residues G74-D76 and their hydrogen-bonded partners, T91-N92, of the β6-β7 shank lie in a region of well defined density. Beyond the sharp turn at P93 (N94-D97), side chain density becomes significantly more diffuse or non-existant. Due to the absence of side chain density for K96, alanine was substituted at this position in this final model.

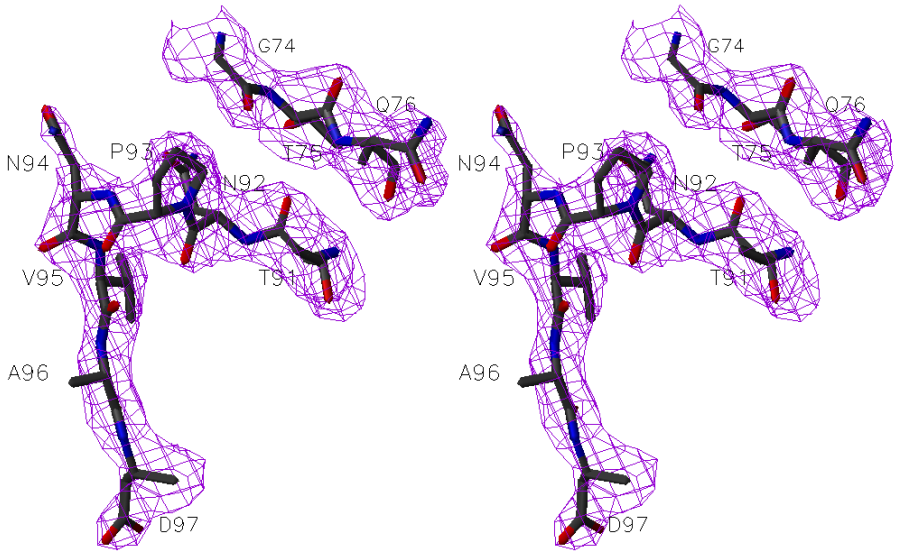

Fig. 17 Electron density adjacent to the disordered C-terminus of IscA

The lack of electron density attributable to Fe might simply be a result of the fact that this area of the structure, which presumably supplies the Fe ligands, is disordered. Moreover, we were unable to detect Fe in the crystal by X-ray fluorescence (data not shown). However, we cannot entirely exclude the possibility that the crystallization conditions were incompatible with iron binding. An alternate explanation, and the one we favor, is that formation of the elliptical cavity in the oligomeric form of

IscA precludes access by two of the four iron ligands (C99,C101) into the pocket that houses both C35 and E82.

At solution concentrations which produce dissociation of the IscA oligomer into either the IscA dimer or tetramer B, C35 would be exposed on the external scaffold and the CGCGESF stretch would be able to wrap around the edge of the former, tetrameric cavity and arrange C99 and C101 into a conformation necessary for Fe ligation. Consistent with the idea that the tetrameric arrangement in the crystal precludes Fe binding to IscA is recent data which demonstrate that the affinity of IscA for Fe decreases at protein concentrations which produce higher-order oligomers (Ding et al., unpublished observations). In contrast, our inability to locate Fe in the native crystal structure is inconsistent with the model proposed for cyanobacterial IscA1: Fe or 2Fe-2S cluster binding sites are maintained at an interface between dimers by two protein ligands (C99, C101) contributed from each monomer (Wollenberg, Berndt, Bill, Schwenn and Seidler 2003). In this scenario, which does not require participation of C35 and E82, monomers present at opposite corners in the elliptical cavity of a tetramer A solution species would provide C99/101 residues from CGCGESF stretches which, according to the direction of the last visible C-terminal residues in opposite chains, are in line to meet and coordinate Fe at a solvent exposed site just outside the cavity center. If this latter represents the true mode of iron binding, however, we would expect to observe bound Fe in the crystal structure as neither crystal packing nor IscA oligomerization is anticipated to interfere with this proposed mechanism.

Comparison of Iron-Sulfur Scaffolds IscA and IscU

Although *in vitro* kinetic and steady state spectroscopic data suggest that IscU/IsU and IscA/IsA assemble solvent-accessible, labile Fe-S clusters and transfer these clusters to apo-ferredoxin at similar rates, there are noteworthy differences in primary sequence, function, and fold. For example, IscA/IsA and IscU/IsU are each highly conserved yet share no significant sequence homology, IsA binds Fe-S clusters with a higher affinity than IsU, and IsA recognizes a binding site on the target ferredoxin distinct from that recognized by IsU (Wu and Cowan 2003). Whereas the high degree of conformational flexibility observed for apo/holo-IscU has been attributed to a series of highly mobile hydrophobic side chains (Bertini, Cowan, Del Bianco, Luchinat and Mansy 2003), a rigid and extensive hydrophobic network imparts stability to the core of monomeric IscA. In contrast to the global fluidity of IscU, only a few residues within the cysteine pocket or the C-terminal tail were significantly disordered in native IscA. Beyond the dynamic features which distinguish these structures, IscA and IscU diverge in both secondary structural content and, insofar as a three-dimensional representation of IscU could be obtained, the organization of these secondary structural elements. However, the disorder present in the structures of both IscA and IscU are consistent with a role for these proteins in the assembly and transfer of transient Fe-S clusters to various Fe-S target proteins. This hypothesis is supported by the observation that all of the three conserved cysteines are located in mobile loop regions of IscA and IscU, at least one of the predicted Fe-S cysteine ligands could not be visualized in either structure, and the remaining cysteines were impossible to position precisely within the putative Fe-S binding regions of native IscA or apo/holo IscU. In addition, neither IscA nor IscU

possess the degree of rigidity characteristic of Fe-S cluster or metal binding sites observed for the majority of known metallochaperone or metalloenzyme structures, many of which bear the common ferredoxin-like or Rossman-type folds (Rees 2002). These Fe-S complexes, which function primarily as redox-labile cofactor centers for catalysts or oxygen sensors, are structurally versatile and, with few exceptions, capable of rearrangement with minimal, highly localized conformational changes in the protein ligands that maintain the Fe-S cluster.

PART B

ACETYL-COA CARBOXYLASE; CARBOXYLTRANSFERASE

CHAPTER IV

INTRODUCTION

Perspectives on an Escalating Public Health Crisis: the Emergence of Antimicrobial Resistant Strains of Major Nosocomial Pathogens *S. aureus* and *E. coli*

A survey of Centers for Disease Control and Prevention reports over the last quarter century indicate that the prevalence rates of severe, multi-drug resistant (MDR) bacterial infections, including those caused by pathogens previously confined to the hospital setting, have undergone alarming increases in both intensive care units and community populations (2004; Menichetti 2005). Chief infective organisms, comprising representatives from gram-positive (*S. aureus*, *Streptococcus pneumoniae*) and gram-negative (*E. coli*), *Pseudomonas aeruginosa*) bacterial subdivisions, have ultimately developed resistance to successive generations of clinically-useful antibiotics. The severity of this microbial threat is underscored by the recent emergence of vancomycin-intermediate and resistant clinical isolates of methicillin-resistant *S. aureus* (MRSA), strains responsible for a preponderance of severe nosocomial illnesses including ventilator-associated pneumonia, surgical site infections, and osteomyelitis (Menichetti 2005). Notwithstanding concerns regarding the narrow therapeutic window associated associated with vancomycin treatment, the potential for high-level resistance in MRSA threatens to remove a last-resort therapy for diseases associated with this pathogen.

Similarity in both chemical structure and mechanism of action characterizes contemporary antimicrobial classes since many of these classes stem from multiple

derivatizations of preexisting parent compounds (Powers 2004; Spellberg, Powers, Brass, Miller and Edwards 2004). These derivatives were designed to preserve the core pharmacological properties of natural antibiotics and to simultaneously elude rapidly evolving resistance mechanisms (Powers 2004; Spellberg, Powers, Brass, Miller and Edwards 2004). An unfortunate outcome has arisen from this strategy: a limited number of cellular targets and accompanying mechanisms of action characterize frontline antimicrobial therapies, most of which are currently inefficacious towards a significant proportion of hospital-acquired pathogens. In addition, the MDR phenotype in common nosocomial microbes (such as MRSA) is significantly exacerbated in response to selection pressure elicited by antimicrobial overadministration (Dzidic and Bedekovic 2003; Lowy 2003). The development of pharmaceuticals against novel bacterial targets therefore presents a compelling medical need (Shah 2005).

The Potential for Novel Antimicrobial Targets in the Fatty Acid Biosynthetic Pathway

A subset of enzymes which catalyze bacterial type II fatty acid biosynthesis (fasII), a pathway set apart from the mammalian type I system by virtue of its requirement for de novo fatty acid production and the structural divergence of its key constituents, represent strong candidates for antimicrobial drug design (Heath, Yu, Shapiro, Olson and Rock 1998; Campbell and Cronan 2001; Marrakchi, Zhang and Rock 2002). Validation of the bacterial fasII system as a potentially fruitful pathway for the selection of novel targets is provided by the recent discovery that clinical anti-tubercular agents isoniazid and ethionamide and the broad-spectrum antibacterial triclosan

selectively inhibit the enoyl-ACP reductase-mediated reduction step of the fasII elongation cycle (Banerjee, Dubnau, Quemard, Balasubramanian, Um, Wilson, Collins, de Lisle and Jacobs 1994; Heath, Yu, Shapiro, Olson and Rock 1998). Additional fasII-pathway antimicrobials cerulenin and thiolactomycin block beta ketoacyl-ACP synthase (KAS) enzymes responsible for fatty acid chain condensation (D'Agnolo, Rosenfeld, Awaya, Omura and Vagelos 1973; Hayashi, Yamamoto, Sasaki, Kawaguchi and Okazaki 1983). However, the design of enoyl-coA reductase and KAS inhibitors across bacterial species is complicated by the presence of orthologous enzymes with multiple isoforms and/or variable substrate specificities (Marrakchi, Zhang et al. 2002). In this regard, the widespread conservation of bacterial acetyl-coA carboxylase (ACC), an essential enzyme which generates the malonyl-CoA precursor required for the subsequent condensation steps of de novo fatty acid synthesis, accents ACC as a more attractive fas-II pathway target. The potential for development of potent ACC inhibitors is demonstrated by the broad-spectrum activity of the antibiotic Moiramide B and its derivatives, the pyrrolidinediones (Freiberg, Brunner, Schiffer, Lampe, Pohlmann, Brands, Raabe, Habich and Ziegelbauer 2004; Pohlmann, Lampe, Shimada, Nell, Pernerstorfer, Svenstrup, Brunner, Schiffer and Freiberg 2005). Other compounds, including several classes of well-established herbicides, the aryloxyphenoxypropionates (AOPPs) and cyclohexanediones (CODs), and a synthetic bisubstrate analog represent additional ACC-selective inhibitors (Burton, Gronwald, Somers, Connelly, Gengenbach and Wyse 1987; Levert and Waldrop 2002).

The Development of Bacterial Acetyl-CoA Carboxylase Inhibitors Holds Promise for Antimicrobial Drug Design

Recent evidence attests that the ACC reaction, or biotin-dependent carboxylation of acetyl-coA, is the rate-controlling step of the fas-II pathway from eubacteria through metazoa (Ha and Kim 1994; Page, Okada and Harwood 1994; Davis, Solbiati and Cronan 2000). In bacteria engineered to secrete excess fatty acyl chains, ACC overexpression markedly increases the overall rate of lipid biosynthesis (Ha and Kim 1994). Similar results, in the form of significant flux control coefficients, are obtained through selective herbicide inhibition of orthologous ACC from leaf chloroplast (Page, Okada et al. 1994). Likewise, the degree of specific, ribozyme-mediated disruption of ACC function correlates directly with the extent of fatty acid synthesis inhibition in mammalian preadipocyte cultures(Davis, Solbiati et al. 2000).

In vivo ACC activity requires the following protein constituents: biotinoyl carboxyl carrier protein (BCCP), biotin carboxylase (BC), and carboxyltransferase (CT). These components participate in the following partial reactions:

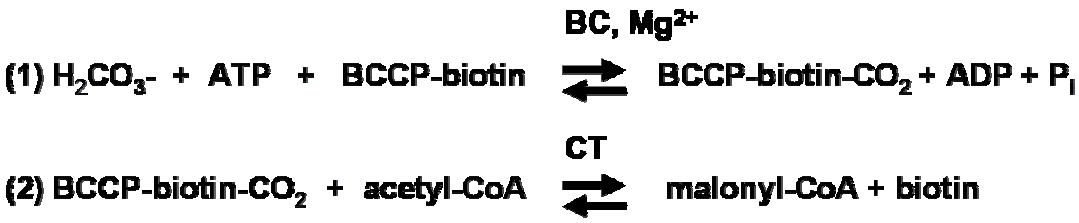

Along the ACC reaction pathway, the biotinoylated mobile arm of BCCP shuttles the biotin cofactor from the site of BC-mediated, ATP-dependent carboxybiotin production (1) into the site of CT-mediated CO2 transfer from carboxybiotin to acetyl-CoA (2). In eubacteria, protozoa, and plant chloroplasts, ACC activity arises from a multi-subunit assembly (prokaryotic ACC) of monomeric biotin-BCCP, dimeric BC, and

heterotetrameric ($\alpha 2\beta 2$) CT or, as expressed in fungi, animals, and plant cytosol, each of these subunits function as distinct domains within a single polypeptide (eukaryotic ACC) (Cronan and Waldrop 2002; Barber, Price and Travers 2005). The two-step carboxylase reaction mechanism and the structural organization of the ACC multienzyme into distinct BC, BCCP, and CT components is shared among members of the biotin-dependent enzyme family, including propionyl-CoA carboxylase (PCC), transcarboxylase (TC), glutaconyl-CoA decarboxylase (GCD), and methylcrotonyl-CoA carboxylase (MC) (Jitrapakdee and Wallace 2003). In conjunction with the lack of primary sequence conservation observed between the prokaryotic and eukaryotic forms of ACC, the major differences in multi-enzyme subunit composition are features which can be exploited to inhibit specific partial reactions of bacterial ACC without disrupting function of the mammalian homologue.

Evidence of a Gene Regulatory Role for the Carboxyltransferase Subunit of Bacterial Acetyl-coA Carboxylase

Although short and long-term regulatory processes which modulate ACC expression and activity are well characterized for the mammalian enzyme, elucidation of the corresponding mechanisms for its prokaryotic counterpart are still poorly understood (Cronan and Waldrop 2002). In contrast to the traditional genomic organization of central metabolic pathway genes into a discrete bacterial operon, ACC subunit genes exist in three physically segregated transcriptional units (Li and Cronan 1992; Li and Cronan 1992; Li, Rock and Cronan 1992). Two of these units produce dicistronic mRNAs which encode either BCCP/BC or the CT-β subunit in conjunction with dihydrofolate

synthetase-folylpolyglutamate synthetase (folC). The third generates a monocistronic transcript encoding CT-α. Since ACC subunits do not undergo cotranslation from a polycistronic mRNA, a major unresolved question concerns the control mechanisms which allow individual subunits to achieve proper stoichiometry in the ACC complex. Transcriptional analysis demonstrates cellular growth-rate dependent mRNA synthesis rates for all *E. coli* ACC subunit genes and reveals independent transcriptional modulation of the BCCP-BC (AccBC) operon and the CT-α (AccA) or CT-β (AccD) gene promoters(Li and Cronan 1993). Relative to wild-type *E. coli*, AccA/AccD transcripts accumulate significantly in transformants containing high-copy number plasmids expressing AccA or AccD, but only weak induction of AccB/AccC mRNA synthesis is observed in bacteria harboring AccBC on the same vector (James and Cronan 2004). This latter observation led to the discovery that BCCP mediates transcriptional repression of the AccBC operon. However, since BCCP was reported to be incapable of binding to the AccBC promoter, the DNA-binding factors and cis regulatory elements which operate downstream of BCCP to control AccBC mRNA expression remain to be established.

Studies of prokaryotic ACC gene expression and activity in chloroplasts, the site of lipid biosynthesis in plants, reveal striking parallels with the *E. coli* enzyme. Phylogenetic evidence indicates that plastidic ACC subunit genes are derived from a cyanobacterial endosymbiont and, excepting chloroplast-encoded AccD, have since undergone transfer to the nuclear genome (Martin, Stoebe, Goremykin, Hapsmann, Hasegawa and Kowallik 1998). All plastidic ACC subunits align with high sequence homology (44-54% identity in Arabidopsis thalania) and conserved secondary structure

(based on topological prediction against Glycine max) over each of the full length *E. coli* sequences. Despite genomic compartmentalization, plastidic ACC mRNA levels are controlled according to the demand for seed oil production and maintain a precise molar ratio throughout Arabidopsis embryogenesis (Ke, Wen, Nikolau and Wurtele 2000). Analogous to the bacterial system, the gene regulatory mechanisms which allow balanced, prokaryotic ACC mRNA expression in plants are largely unexplored.

To date, several lines of evidence suggest that the CT-β subunit directly modulates transcription. The plastidic orthologue of bacterial AccD, whose protein coding sequence contains the invariant N-terminal, zinc binding consensus C-x2-C-x15-C-x2-C in eubacteria, photosynthetic protozoa, and plants, was first classified as the zinc-finger protein A (zfpA) (Sasaki, Nagano, Morioka, Ishikawa and Matsuno 1989). zfpA (AccD) was proposed to act as an immediate response, gene regulatory factor in chloroplasts since light stimulates production of plastidic AccD mRNA in the absence of de novo protein synthesis. The observation that deletions within either the *E. coli* AccD gene or its upstream promoter markedly truncate FolC expression from a plasmid-borne AccD-FolC operon suggests that CT-β might modulate *E. coli* gene expression in analogous fashion (Bognar, Osborne and Shane 1987).

The conserved zinc finger motif of CT-β, in addition to a proposed gene regulatory role, is required for the CT half-reaction of plastidic ACC (Kozaki, Mayumi and Sasaki 2001). Reconstitution of pea CT after removal of the CT-α and CT-β sequences lacking conservation with the *E. coli* orthologue, which comprises a large N-terminal segment upstream of the Zn finger consensus in plastidic CT-β, exhibits wild-type activity. Further N-terminal truncation through the Zn finger motif, however, completely

abrogates CT activity and mutagenesis of the four individual cysteines to alanine produces an enzyme which exhibits <20% wild-type activity (Kozaki, Mayumi and Sasaki 2001).

Purpose

The purpose of this study was to determine the three dimensional structure of the CT subunit of bacterial ACC, a potential antimicrobial drug target. Since CT was crystallized in the presence of a bisubstrate analog inhibitor, the structure was anticipated to reveal the mode of inhibitor binding and to provide insight into the catalytic mechanism. It was additionally anticipated that the active site structure would help to elucidate the inhibitory mechanism of the pyrollidine diones, a new class of antimicrobials specific for the CT subunit of ACC.

CHAPTER V

MATERIALS AND METHODS

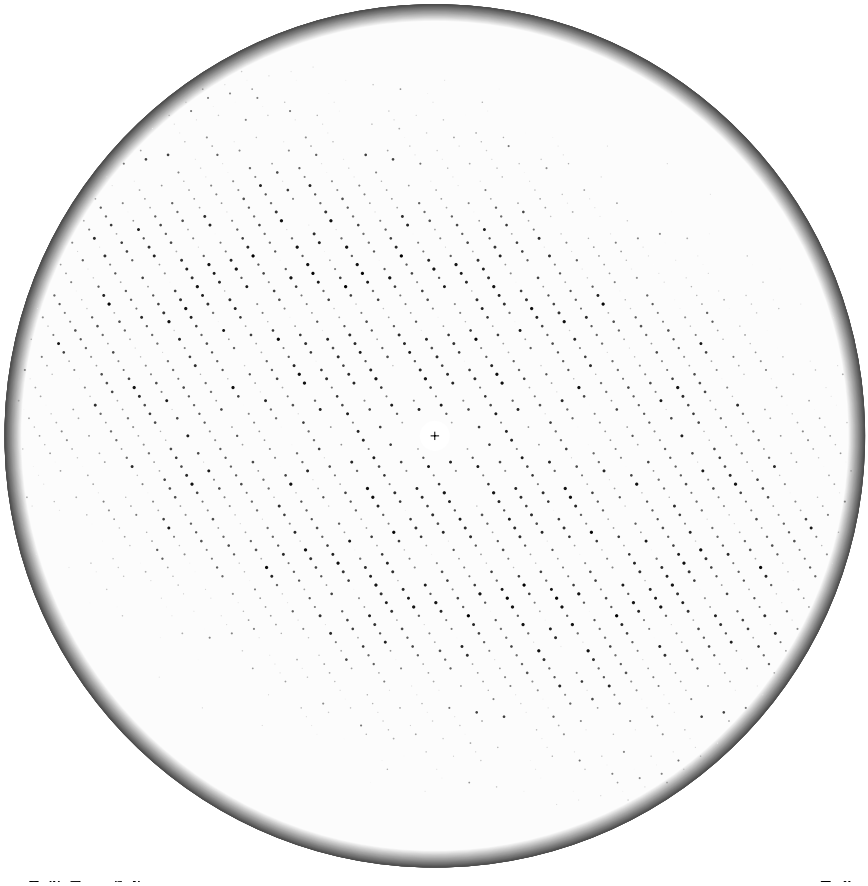

Fig. 18 Simulated precession image of *Sa* CT diffraction

Structure Determination and Refinement

Sa CT purification, crystallization, and data collection were performed at Pfizer Global Research and Development, Ann Arbor, Michigan. Diffraction images were processed

and scaled using the Denzo/HKL suite (25). A precession image on the 0,k,l zone of reciprocal space was simulated from the scaled intensity data and presented in Fig. 18. Reflections on l and k are respectively aligned on the short and long axes of the page. Odd reflections on k are absent due to the presence of a screw axis along the direct axis y of the C2 lattice. Data collection statistics are shown in Table. 3.

Table 3 : X-ray Data Collection Statistics

	Sa **CT**	*Ec* **CT**
resolution (Å)	**50.0-1.98**	**30.0-3.2**
total/unique reflections	**273,345/90,018**	**183,454/23,565**
completeness (%)	**98 (82)**	**100 (100)**
redundancy	**3.0 (2.7)**	**7.8 (8.0)**
I/σ	**17.5 (3.4)**	**26.6(4.1)**
Rsym(%)	**6.0 (29.3)**	**6.8 (41.2)**

The structure of *Staphylococcus aureus* carboxyltransferase (*Sa* CT) was solved by molecular replacement in CNS with a dimeric poly-alanine search model derived from the *Propionibacterium shermanii* 12S transcarboxylase (*Ps* 12S) hexamer (PDB id 1ON3, chains A, D). A monomer of the search model corresponds to a tandem domain repeat and each of the structurally homologous domains shares <15% sequence identity with the α and β subunits of *Sa* CT. The search model (corresponding to an $\alpha_2\beta_2$ tetramer) was positioned in the asymmetric unit to give a correlation coefficient two standard deviations above the mean. Placement of a single dimeric model is consistent with the non-crystallographic symmetry of the Patterson and a Matthews coefficient (Vm= 2.4 $Å^3$/Da) in the generally observed range. After rigid body, energy minimization, and simulated annealing refinement in CNS (Rfree=53, R=52) of the poly-alanine model, a

sigmaA-weighted, 2fo-fc electron density map calculated over the full resolution range (50-1.98Å) revealed interpretable side chain density for a few conserved residues in the central core of the model.

A non crystallographic symmetry matrix, assigned with the assumption that the monomer pseudo two-fold of the 12S search model corresponds to an αβ dimer pseudo two-fold in the *Sa* CT tetramer, was used to calculate an averaged, solvent flattened electron density map with DM in CCP4. The map revealed clear side chain electron density at or near the dimer interface. Automated chain tracing and refinement with ARP-wARP (Perrakis, Harkiolaki, Wilson and Lamzin 2001) (CCP4) increased the extent of an initial model (from 11% to 80% of the protein) and resulted in an and $R_{work}/R_{(free)}$ of 20/26. Following further cycles of model building in O and refinement in Refmac 5 (CCP4) over the entire resolution range, the final model of *Sa* CT has an $R_{work}/R_{(free)}$ of 18.9/21.0 and contains 92% (1120/1224) of the full length sequence, 2 Zn^{2+}, and 583 waters (Table 3). The remaining 8% of *Sa* CT localizes to a 22-residue disordered stretch at the far N-terminus of the β subunit and to a 10 residue gap between solvent-exposed helices at the N-terminus of α. A simulated annealing composite omit map calculated in CNS and contoured at 1σ reveals electron density in the active site that has been modeled as the biotin heterocycle.

A molecular replacement strategy for *Ec* CT was subsequently initiated with a polyalanine search model derived from the refined *Sa* CT structure. Dimeric and tetrameric search models were tested in each of several possible hexagonal space groups. A solution (using Molrep (CCP4)) was obtained in $P6_522$ (Vm= 5.0 $Å^3$/Da, 75% solvent) with the αβ dimer as a search model. In this space group, crystallographic symmetry

operators generate the biological heterotetramer from a single αβ dimer in the asymmetric unit. One cycle of rigid body, energy minimization, and simulated annealing refinement in CNS produced a map with interpretable side chain density for approximately 80% of the *Ec* CT primary sequence (Rfree=46, R=42). In conjunction with model building in O and overall isotropic B-factor refinement in CNS, further cycles of energy minimization and simulated annealing refinement were conducted until Rfree decreased below 30%. At this stage, seven water molecules were added and a final round of B-group and simulated annealing refinement was performed (Table 4). The backbone trace of the final *Ec* CT model (Rfree=29, R=25) superposes well (rmsd=1Å) with the Sa CT model and lacks density in similar regions of the structure. There are additional poorly defined stretches encompassing residues 88-98 and 234-238 of the β monomer.

Table 4 **Refinement Statistics**

	Sa CT	*Ec* CT
resolution range (Å)	50-1.98	30-3.2
number of reflections	80,987	22,030
sigma cutoff	none	none
R factor (%)	18.9	24.6
R free (%)	21.0	29.3
number of refined atoms:		
protein	8,689	4,275
water	583	7
Zn2+	2	1
average B factors (Å2):		
protein	38.4	79.9
water	42.8	44.6
Zn 2+	40.1	78.6
Overall	38.7	79.8
B from Wilson plot	31.7	N/A
rms deviations:		
bonds (Å):	0.02	0.01
angles (°):	1.4	1.4
ramachandran plot		
disallowed (%)	0.1	0.0

CHAPTER VI

RESULTS

Overall Fold

The crystal structures of the carboxyltransferase components of acetyl-CoA carboxylase from *S. aureus* and *E. coli* were solved to resolutions of 2.0 and 3.2Å, respectively. Both structures confirm the $\alpha_2\beta_2$ heterotetrameric assembly determined by gel-filtration and sedimentation equilibrium analysis of the purified *E. coli* enzyme (Guchhait, Polakis, Dimroth, Stoll, Moss and Lane 1974). The bacterial CT's share 52% sequence identity, and the tetramers superimpose with a rmsd of 1Å over 93% of the backbone trace (unless otherwise noted, the *E. coli* residue numbering employed throughout the text refers to residues conserved between both species). The overall structure of the tetramer is a truncated rectangular pyramid with its base 72Å x 88Å, apex 23Å x 34Å, and height 52Å (Fig.1a,b,d). The oligomer is a dimer of dimers related by a two-fold axis that runs through a central cavity that gradually narrows from a 13Å diameter opening to a solvent inaccessible surface at a depth of 23Å. Two distinct interfaces are generated by structurally-homologous, wedge-shaped α and β monomers that occupy roughly equivalent volumes at the four corners of the pyramid (Fig. 19 a,b). The first consists of a "weak" αβ interface (~4000Å^2 of buried surface) situated on the vertical plane bisecting the short axes of the pyramid (Fig. 19 c,d). The second entails a "strong" αβ interface (~9000Å^2 of buried surface) in which the triangular faces of the monomers are juxtaposed on a 60° incline (Fig. 19 e,f).

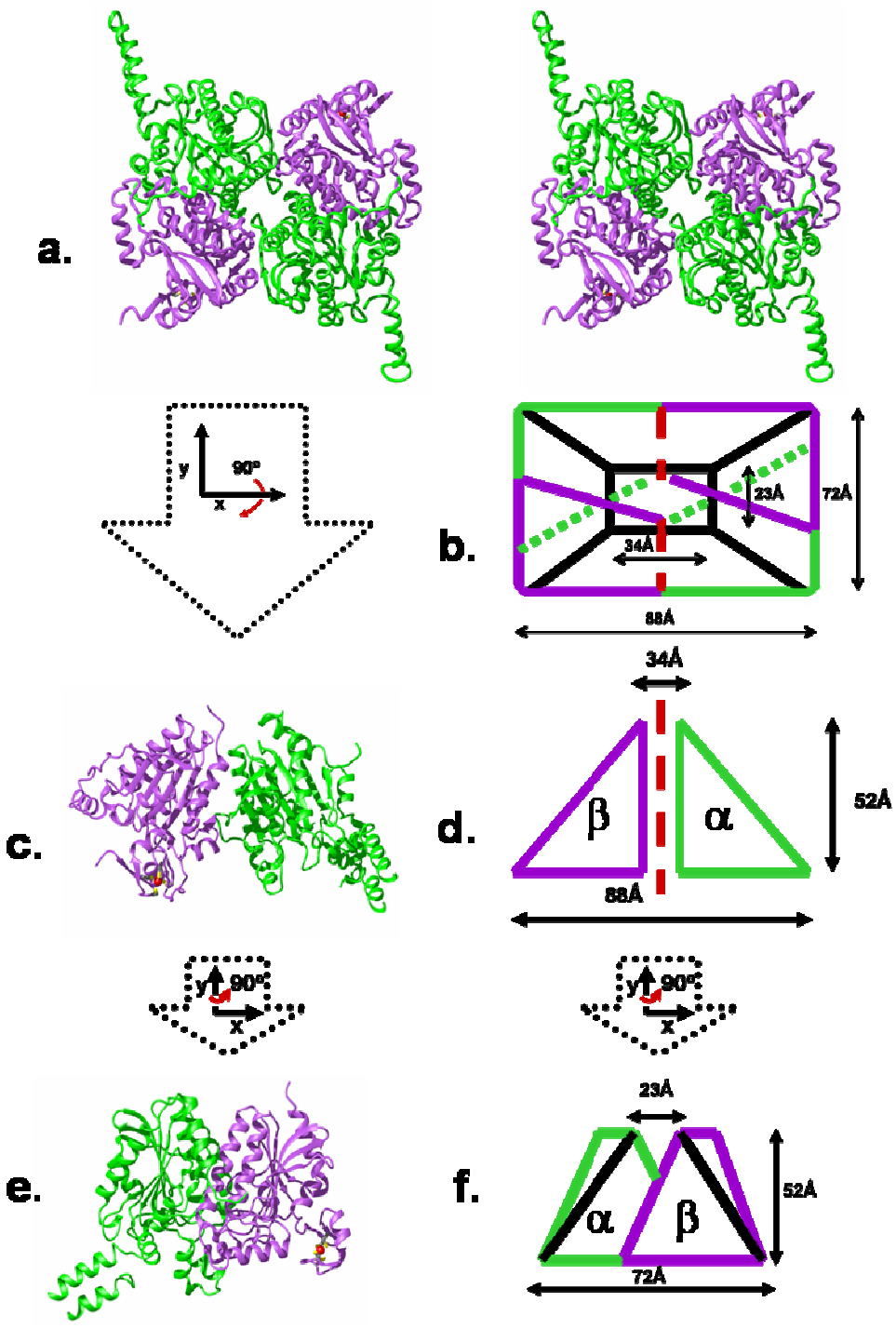

Fig. 19 The overall fold of *Sa* CT

The structurally-similar α and β monomers (A and B) possess an α/β spiral core composed of a long, twisted and tapered 7-stranded mixed β sheet (Aβ1-5/Bβ5-9, Aβ6/Bβ11, Aβ8/Bβ13) orthogonal to a short, 2-stranded parallel β platform (Aβ5/Bβ10, Aβ7/Bβ12) (Fig. 20).

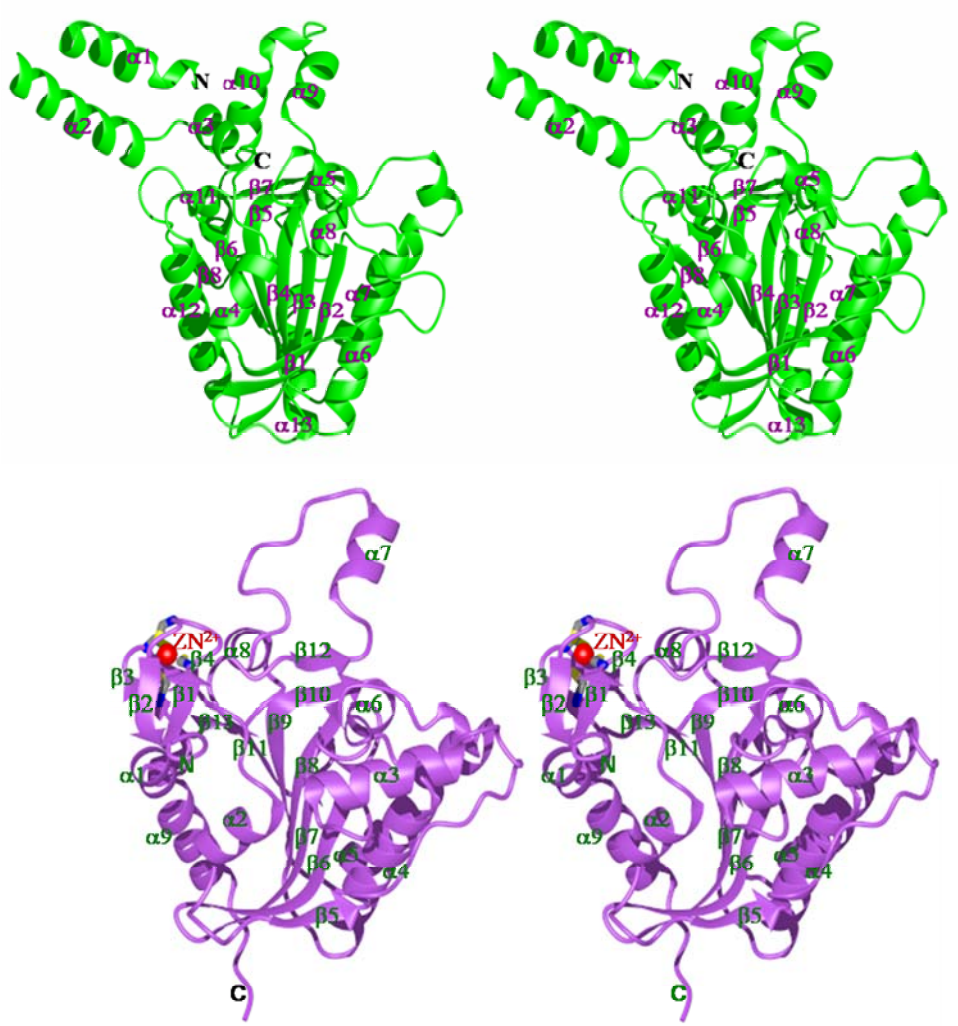

Fig. 20 The α (green) and β (purple) monomers of bacterial CT (in stereo)

The 7-stranded β sheet is flanked by helical regions (Aα12/Bα9 and Aα4/Bα2) and a 3-helix bundle of Aα6/Bα4, Aα7/Bα5, Aα8/Bα6. These helical elements constitute

pseudo-symmetrical edges of the triangular face of the wedge. Both sets of helices converge toward the apex of this triangle and the 3-helix bundle provides the primary scaffold for the 2-stranded platform at its base. The structure-based sequence alignment in figure 21 highlights the extensive structural homology of 1) the spiral α/β monomer fold to enoyl-CoA hydratase (crotonase) and 2) the presence of an oxyanion hole (G204-G205) for CoA-thioenolate stabilization as described for other members of the crotonase superfamily. Both of these elements, which are maintained through divergent evolution, place the bacterial CT subunits into this enzyme subcategory (Gerlt and Babbitt 2001). This classification was originally predicted by Murzin on the basis of sequence alignments (Murzin 1998). Figure 21 is color coded as follows: *E. coli* / *S. aureus* α (light green), *Streptomyces coelicolor* (*Sco*) domain 1 (dark green), *Ec*/*Sa* β (light purple), Sco domain 2 (dark purple), and crotonase (blue). Sequences are numbered according to the *E. coli* α/β monomers and secondary structural elements corresponding to the *S. aureus* α/β monomers (above the alignment) or crotonase (below the alignment) are color coded according to the scheme employed for the *E. coli* / *S. aureus* monomer or crotonase sequences. Secondary structural elements within the structurally-homologous spiral core domains of *E. coli* / *S. aureus* monomers and crotonase is outlined. Within the outlined region, residues that constitute the conserved oxyanion holes that recognize the biotin ureido enolate or CoA thioenolate intermediates are boxed in black. The invariant cysteinyl zinc ligands in CT β are boxed in red. Residues in *E. coli* α (22-38,41,46,52-53) and *E. coli* β (93-98,285-204) that are not visible or lack clear side chain density are absent or modeled as alanine, respectively.

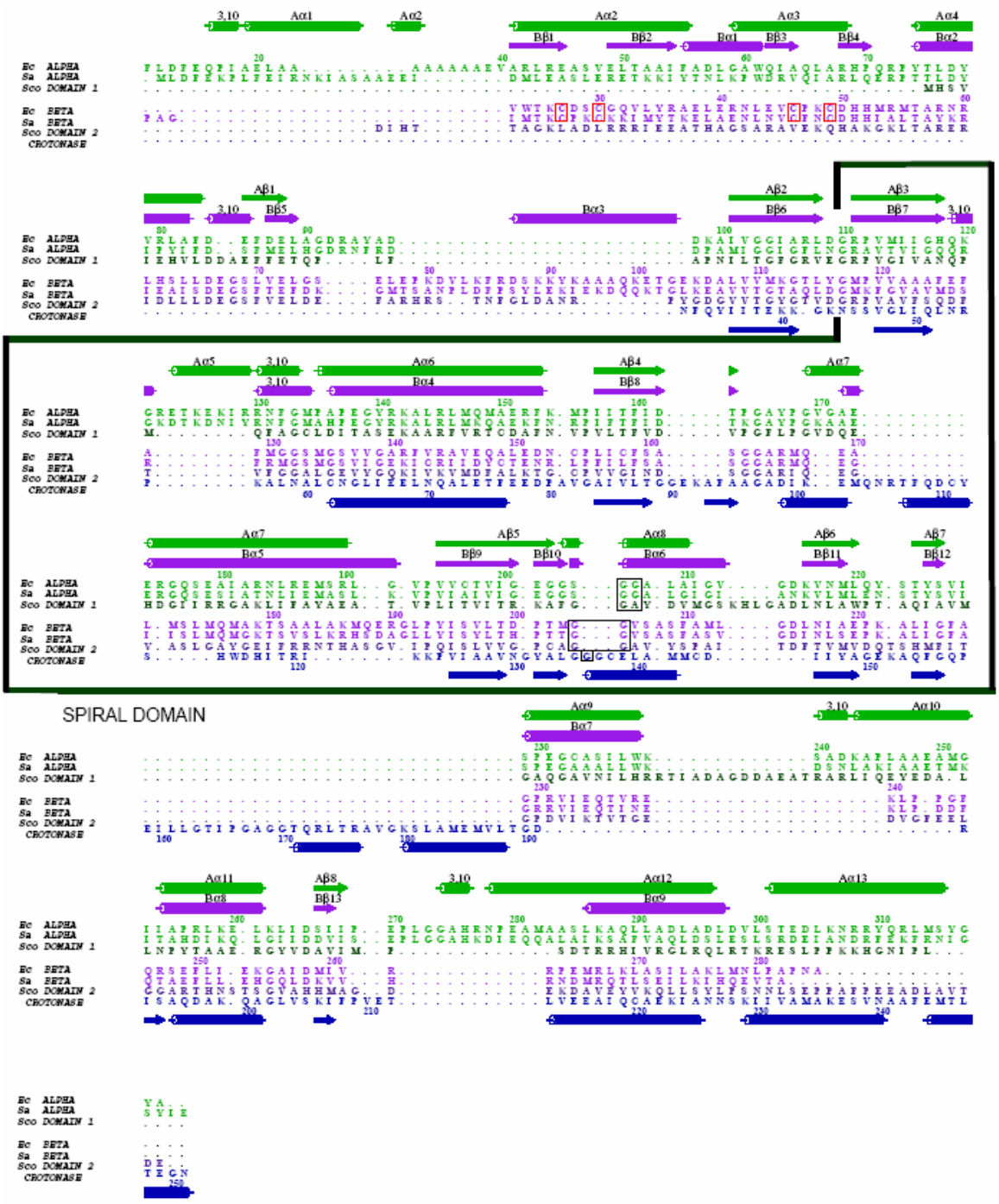

Fig. 21 Structure-based alignment of *Ec* and *Sa* CT α/β with *Sco* CT and crotonase

The Active Site

A "ridges in grooves"-type stacking of conserved hydrophobic residues between the Aα7-8 (I181,L185,L209) and Bα5-6 (L174,M177,A208) helices generates a 6-helix

bundle at the "strong" αβ interface. This packing arrangement orients the triangular faces of dimer partners on a 60º tilt with respect to one another and effectively doubles the length of the β-strand platform by positioning the hairpins from individual monomers on opposite sides of a pseudo two-fold axis (Fig. 22). Since conserved residues found on and surrounding this platform are located in the liganded active sites of other biotin dependent carboxylases, including the substrate-binding clefts of *Streptomyces coelicolor (Sco)/Saccharomyces cerevisiae (Sc)* CT (Zhang, Yang, Shen and Tong 2003; Diacovich, Mitchell, Pham, Gago, Melgar, Khosla, Gramajo and Tsai 2004) and *Propionibacterium*

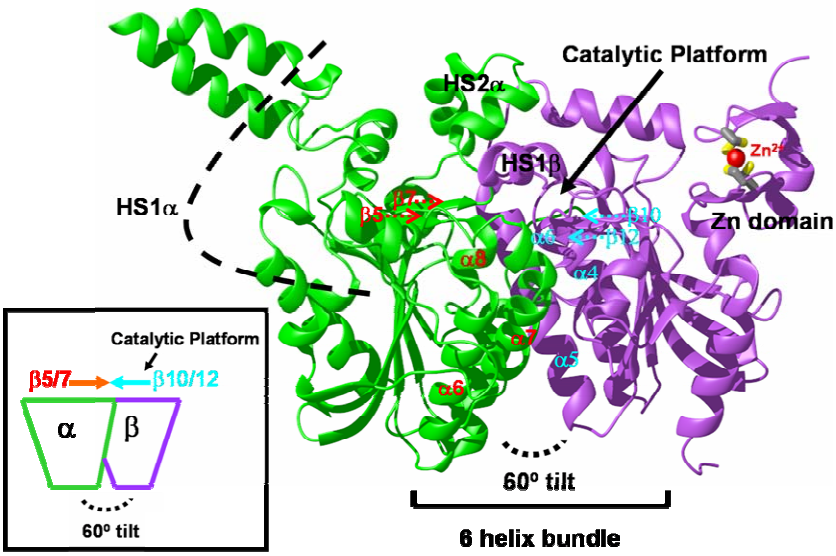

Fig. 22 Structure of the *Sa* CT αβ catalytic dimer

shermanii 12S transcarboxylase (*Ps* 12S)(Hall, Wang, Rivera-Hainaj, Zheng, Pustai-Carey, Carey and Yee 2003), we will henceforth refer to this site as the "catalytic platform" (Fig. 22). The structurally equivalent overall folds of the α and β subunits suggest duplication and divergence of a single ancestral CT subunit gene. However, an

inherent asymmetry in the structural homology of the α and β subunits allows for the creation of distinct biotin and acetyl-CoA-specific subsites. When viewed from a perspective above the αβ interface, the α and β subunits possess structurally disparate motifs that project toward the viewer. As shown in figure 23, four subdomains (2 helical domains from the α-subunit (designated Helical Subdomain (HS) 1α & 2α (HS1α & HS2α), and a Zn binding domain and helical domain from the β-monomer (HS1β)) coalesce to provide a canopy over the catalytic platform where three portals (labeled gaps A B and C in Fig. 23) in the canopy appear to provide active site access.

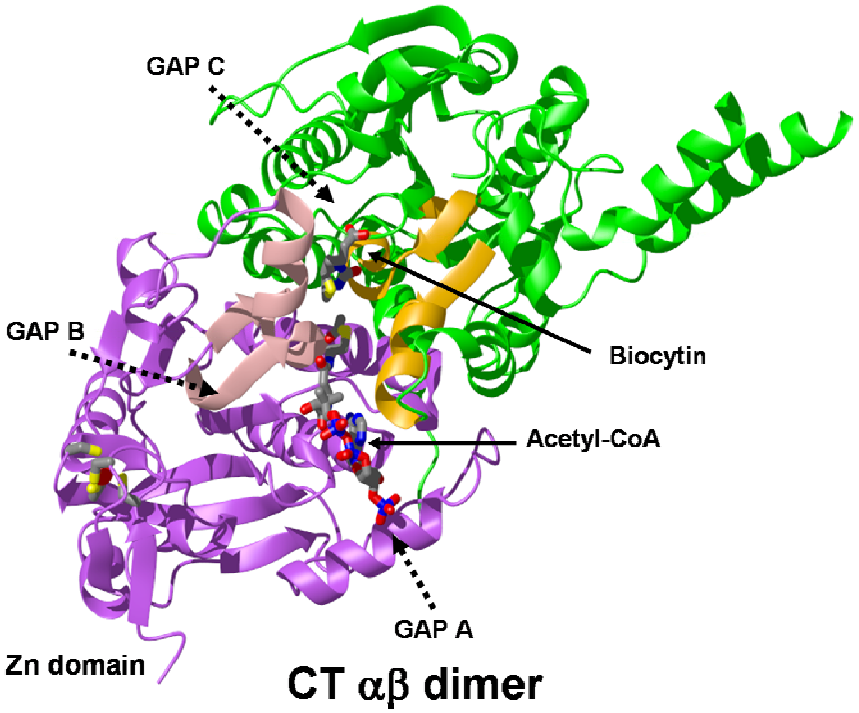

Fig. 23 The pseudo 2-fold, *Sa* CT active site platform in the αβ catalytic dimer

The regions that flank these portals break the symmetry of the active site that would result if the structural homology of the α or β subunits extended over the entire protein. The portals may serve as "traffic control" elements that coordinate active site access for substrates constrained by bulky carrier groups: biotinoyl carboxyl carrier protein and coenzyme A.

Two key conserved residues in the active site, G206 and G207, are located in the consensus sequence 206-GGXXHHH-212 (where X=small residue, H=hydrophobic), which is at the N-terminus of Aα8 (Fig. 21). The peptidic hydrogens of G206 and G207 form a conserved oxyanion hole at the base of this helix that is proposed to stabilize a ureido enolate that forms during decarboxylation of carboxybiotin N1 in the homologous CT subunit of propionyl-CoA carboxylase (PCC) from *Streptomyces coelicolor* (*Sco*) (Zhang, Yang, Shen and Tong 2003; Diacovich, Mitchell, Pham, Gago, Melgar, Khosla, Gramajo and Tsai 2004). Similarly, a conserved oxyanion hole in the β subunit is formed by G204 and G205 at the N-terminus of Bα6 (Fig. 21). The peptidic hydrogens of this glycine pair in the *Sco* PCC structure, which correspond to the conserved oxyanion hole in crotonase, were found to act as hydrogen bond donors to the carbonyl of the methyl-malonyl-CoA ligand (MMCoA) and proposed to stabilize the developing negative charge on the enolate intermediate (Zhang, Yang, Shen and Tong 2003; Diacovich, Mitchell, Pham, Gago, Melgar, Khosla, Gramajo and Tsai 2004).

It is important to note that *Sa* CT was crystallized in the presence of a bi-substrate analog (BiSA) inhibitor that combines features of both substrates: coenzyme A is covalently linked to carboxybiocytin (Fig. 24) (Levert and Waldrop 2002). However, continuous electron density consistent with the intact inhibitor is not apparent (Fig. 25).

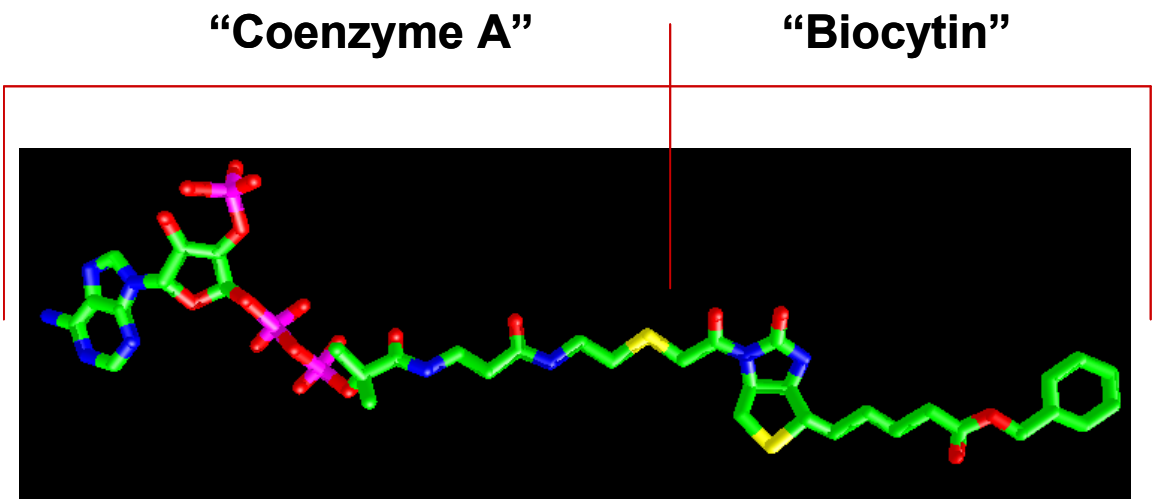

Fig. 24 The Bi-Substrate Analog inhibitor of carboxyltransferase (BiSA)

This absence of density could be a consequence of hydrolysis of the analog in the course of the crystallization, or could simply reflect a lack of specific contacts over the length of the inhibitor in our crystallization conditions.

Inspection of a 2Fo-Fc composite omit map reveals non-protein density that likely corresponds to a portion of the inhibitor in a hydrophobic region of the active site at the central pseudo-two-fold of the catalytic platform (Fig. 25).

Attempts were made to model the inhibitor, however, since density with striking resemblance to the bicyclic ring structure of biotin was evident. BiSA is hydrolyzed and visible in only one active site; in addition to reasonable biotin density, a portion of the phenylated valeric acid and the acyl-CoA moieties were apparent (Fig. 26). Liganded and unliganded active sites superpose with a rmsd of 0.24A and show only minor structural differences. The biotin heterocycle is twisted about the C3-C4 bond into a constrained, puckered conformation which places N3 and C5 above and N1 and C2 below the respective ring planes which would exist in a model of ideal bicyclic mirror symmetry.

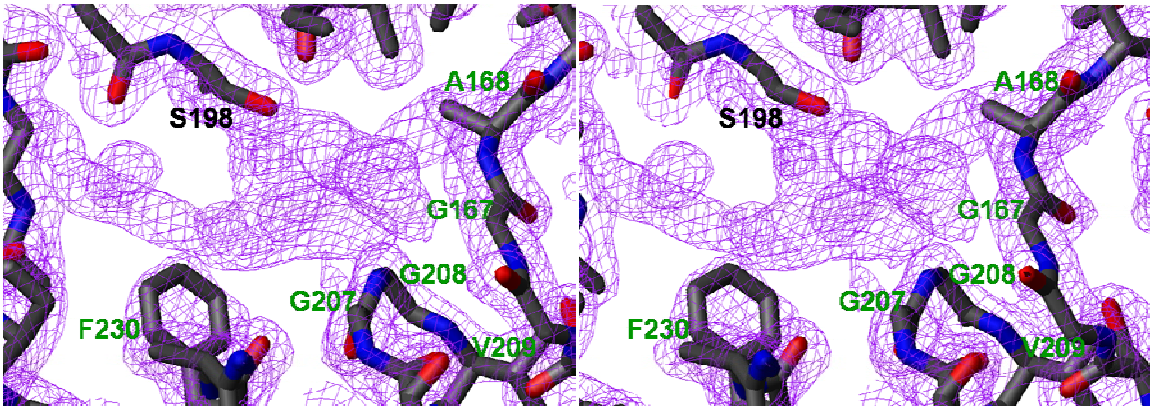

Fig. 25 The *Sa* CT active site (lacking modeled BiSA)

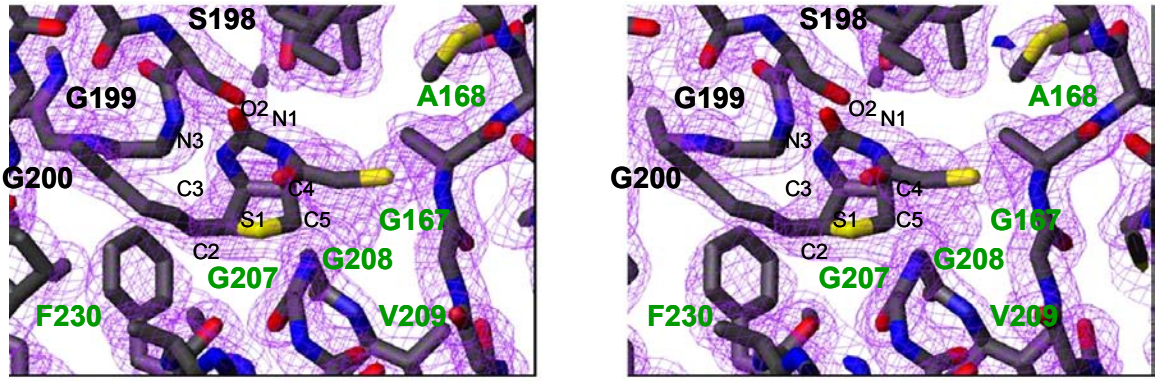

Fig. 26 The *Sa* CT active site (with modeled BiSA)

The C3-C4 bond rests parallel to a hydrophobic cavity which lies along the dimer pseudo two-fold and the vertex described by C3-C4 points directly through the cavity center. The n-termini of the Aα8 and Bα6 dimerization helices are positioned as symmetry equivalent entities with respect to this axis and contribute dipole moments which border biotin at O2' and S1, respectively. The structurally equivalent positions at the n-termini of these helices are conserved in biotin dependent carboxyltransferases such that the consensus for Aα8 is GGXXHHH (where X=small residue, H=hydrophobic) and Ba6 is XXGGXXX. BiSA is surrounded by hydrophobic surfaces emanating from short coils at the base of HS1β and its pseudo-symmetry equivalent in α, a highly conserved bulge (between Bβ8 and Bα5) with the prokaryotic ACC CT β consensus 163-GGARMQE-169

that runs parallel to strand Bβ11 of the catalytic platform, and a short coil between Aβ4 and Aα7 with the prokaryotic ACC CT α consensus GAYPG. The GAYPG consensus represents the pseudo-symmetry equivalent of the GGARMQE loop in β. The sequence and structure (based on *Sc* CT) of eukaryotic ACC also aligns remarkably well in the Bβ8-Bα5 and Aβ4-Aα7 loop regions and suggests that these elements play an essential role in biotin recognition. This hypothesis is supported by the observation that mutagenesis of E169 of *Ec* CT β, a residue conserved in the primary sequence of prokaryotic and most eukaryotic ACCs, results in a catalytically inactive enzyme (Benson and Waldrop, unpublished results).

In the structure of MMCoA/biocytin-bound *Sco* PCC, a biotin-dependent carboxyltransferase whose acyl-CoA substrate differs from acetyl-CoA by the addition of a methyl group, the position of the acyl thioester of MMCoA is in close proximity to the density we tentatively attribute to the bi-substrate analog inhibitor. This density predominantly covers the hydrophobic cavity that presents the helical dipole and oxyanion hole (G207-G208 of Bα6 in *Sa* CT) to the acyl thioester of MMCoA.

The Zinc Domain: Potential for ACC Inhibitor Design

While the overall fold of bacterial CT confirms that it is indeed a member of the crotonase superfamily, a surprising and novel feature of the enzyme is the Zn domain (Fig. 27).

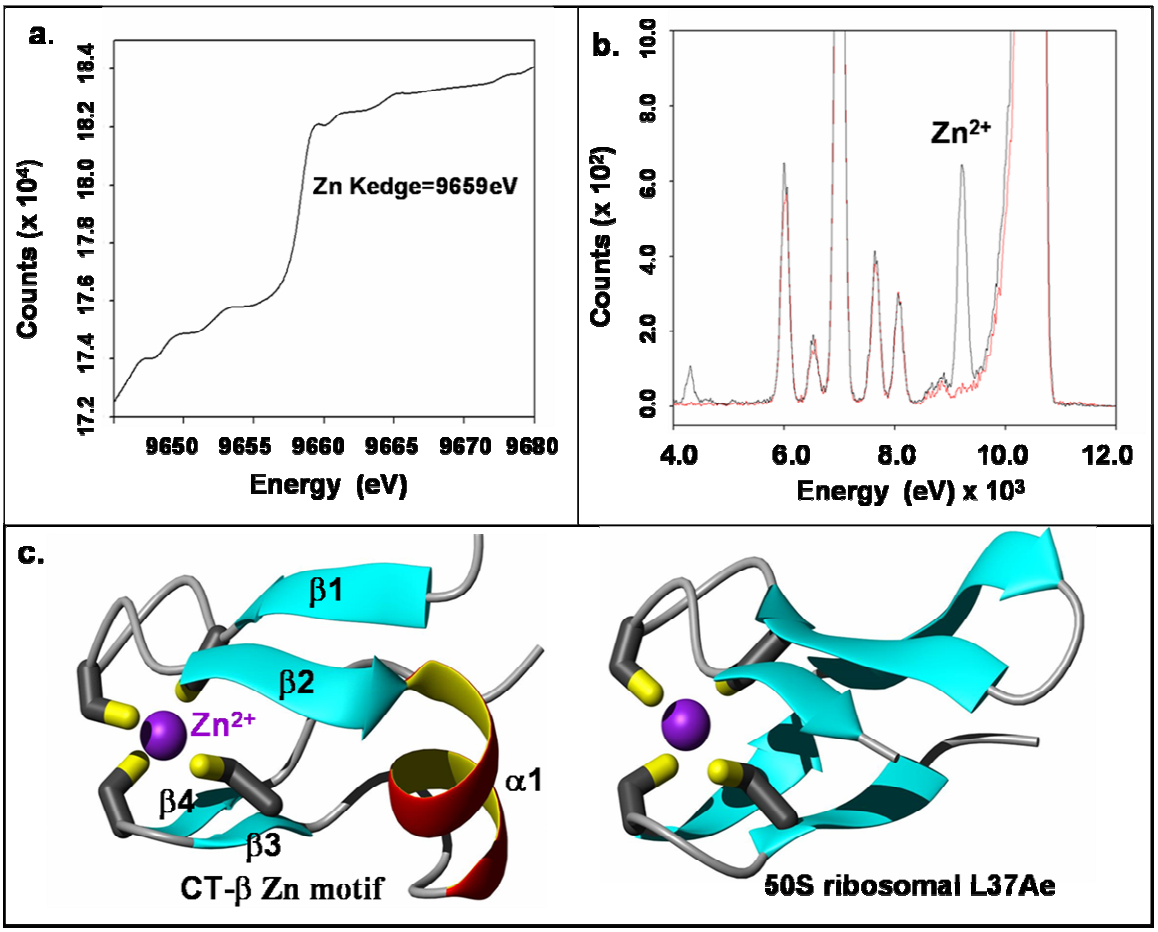

Fig. 27 *Sa* CT binds zinc with an atypical zinc ribbon motif

The discovery that this domain exists in prokaryotic CT alone has potential ramifications for designing pharmaceutical agents that are selective for the bacterial enzyme. Early Fo-Fc maps calculated for the *Sa* CT structure revealed a 20σ peak encapsulated by a tetrahedral arrangement of sulfurs contributed by the cysteine residues that terminate Bβ1(C27)/Bβ3(C46) and those immediately preceding Bβ2(C30)/Bβ4(C49) (Fig.). X-ray fluorescence spectra collected on solution-state and crystalline preparations of *Sa* CT in its apo form demonstrate that the peak corresponds to Zn^{2+} (Fig. 27). Sequence alignment of the CT β primary sequence with orthologous enzymes from eubacteria,

algae, plants, and animals reveals that the cysteine ligands are invariant residues within an independent N-terminal domain that exists in prokaryotic, but not eukaryotic CT. The Zn motif in CT β is an atypical Cys4 "zinc ribbon" that most closely resembles the Zn binding structures observed in ribosomal proteins (Fig.7c; PDB code 1jj2), RNA polymerase II subunits (1i5b) and the basal transcription factors TFIIS(1tfi) and TFIIB(1pft). Unlike the classical motif in which the second sheet is three-stranded and significantly longer than the first (Krishna, Majumdar and Grishin 2003), the fold in CT β bears an intervening helix between two short β hairpins (Fig. 27).

The inner face of the CT β Zn binding domain forms roughly half of an electropositive, hemicircular surface that encompasses residues from both subunits (Fig. 28). Comparison of the electrostatic properties of *Ec*/*Sa* CT with the structurally homologous carboxyltransferases *Sc* CT and *Sco* PCCB reveals that *Ec*/*Sa* CT possess a greater overall net positive charge at pH 7 (*Ec* CT=+4, *Sa* CT=-16, *Sc* CT=-26, *Sco* CT=-42). Zn-domains are commonly associated with DNA binding proteins and preliminary studies using electrophoretic mobility shift assays indicate that *Ec* CT does indeed bind DNA (data not shown). Studies to determine the DNA binding specificity of *Ec* CT are underway.

In addition to nucleic acid binding functions, Zn ribbon structures have also been found to constitute catalytically-essential, active site "lids" in isoleucyl-tRNA synthetase,

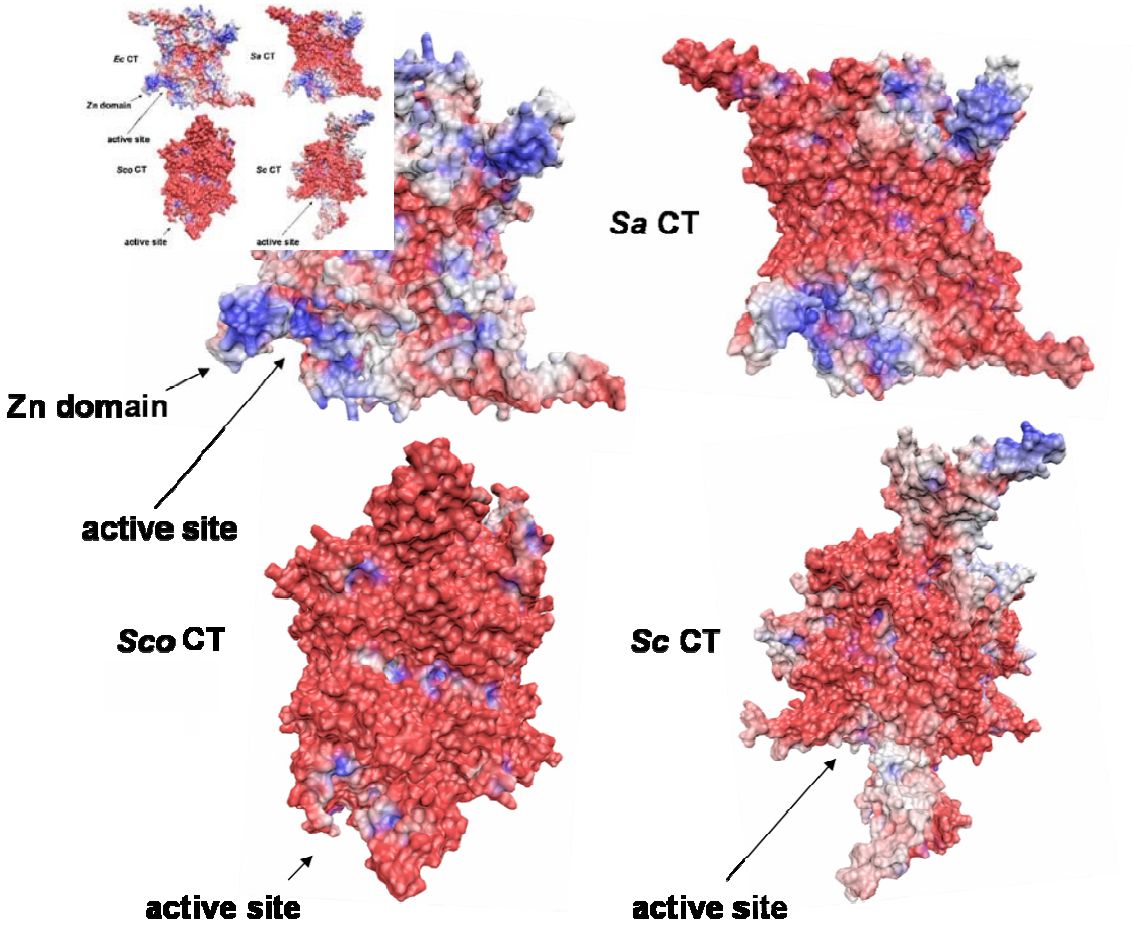

Fig. 28 The Sa/Ec CT active site presents a markedly electropositive surface by comparison to other CT structures

methionyl-tRNA synthetase, and the histone deacetylase silent information regulator 2 (Glasfeld and Schimmel 1997; Sherman, Stone, Freeman-Cook, Brachmann, Boeke and Pillus 1999; Serre, Verdon, Choinowski, Hervouet, Risler and Zelwer 2001; Crepin, Schmitt, Blanquet and Mechulam 2004). In fact, several lines of evidence suggest that the Zn motif in CT β is required for catalytic activity and may also act as an active site "lid". First, the prokaryotic $\alpha_2\beta_2$ CT heterotetramer isolated from plant chloroplast, which aligns over the primary sequence of both bacterial CT subunits (39%/47% identity between pea and Ec CT-β/α), bears the zinc finger consensus C-X_2-C-X_{15}-C-X_2-C (35).

Second, deletion of the Zn finger motif in plastidic CT completely abrogates enzymatic activity, while mutagenesis of the four individual cysteines to alanine produces an enzyme which exhibits <20% wild-type activity (Kozaki, Mayumi and Sasaki 2001). Third, *Ec* CT is inactivated by N-ethylmaleimide (NEM), a compound that covalently modifies sulfhydryls (Blanchard and Waldrop 1998). Since the majority of cysteines in the *Ec* CT structure are buried and no cysteines are present in the active site, these results are consistent with NEM-mediated disruption of the solvent-exposed cysteines in the Zn ribbon domain of CT β. Moreover, malonyl-CoA confers protection against inactivation by NEM, a result which suggests that the Zn domain plays a role in substrate recognition (Blanchard and Waldrop 1998). However, superposition of the *Sa*/*Ec* CT-β monomer with crotonase family members, as well as other biotin dependent carboxylases, including *Sc* ACC and *Sco* PCC, reveals that the acyl-CoA binding site is situated roughly 17Å from the Zn ribbon motif. Although this observed distance alone does not immediately favor a direct contribution of the Zn domain in the catalytic mechanism, we must note that crystal contacts on the outer surface of the Zn domain might maintain the "lid" in an artificially open state in both the *Ec* and *Sa* CT structures. Moreover, a disordered 20+ residue N-terminal stretch in both enzymes immediately precedes the zinc domain and this mobility extends, in the form of higher than average B-factors, through the β1-β4 strands. Since the Zn site is part of a small, independent domain that rests on a short hinge, it is plausible that these disordered and/or mobile residues, many of which are electropositive, order and shift the inner surface of the zinc motif into contact with the electronegative phosphates of the acetyl-CoA substrate. This scenario would mimic the significant mobility observed for the catalytic zinc lid domain of methionyl tRNA

synthetase: although crystal structures of methionyl tRNA synthetase demonstrate a large domain shift, only in the solution state were residues from this domain conclusively shown to interact with substrate (Crepin, Schmitt, Blanquet and Mechulam 2004). Taken together, these observations suggest that the Zn domain may act as a potentially mobile and catalytically-important active site lid for the bacterial enzyme. Moreover, significant variability is observed in the constellation of side chains that project from the inner surface of the zinc domain when the active site structure from the Gram-positive bacterium (*Staphylococcus aureus*) is superposed with *Escherichia coli* (Gram-negative). Since this unique structural feature is both present and variable in Gram-positive vs. Gram-negative bacteria, it may aid in the design and development of pharmaceutical agents that mediate selective, specific inhibition of bacterial enzyme classes.

CONCLUDING REMARKS

Iron-Sulfur Cluster Protein A

The crystal structure of IscA reveals a compact globular domain that tethers a highly mobile C-terminal tail containing residues shown to be involved in Fe-S cluster assembly. It appears that the functional form of IscA is at least dimeric, and that the tethered, flexible C-termini permit the interaction of two IscA monomers with Fe in multiple geometries. In the region of C35, the Hg-binding pocket of tetramer A or the solvent-exposed surface of tetramer B provides adequate space for the insertion of mononuclear iron and/or Fe-S clusters. The crystal packing suggests a model for the polymerization of IscA into the higher order solution states described previously (Ollagnier-de-Choudens, Mattioli, Takahashi and Fontecave 2001;Wu, Mansy, Hemann, Hille, Surerus and Cowan 2002). In conjunction with current models for Fe binding to IscA, our structure suggests that alternate dimeric or tetrameric forms may serve to either enhance or preclude access of the three invariant cysteine residues to Fe or Fe-S ligands.

Acetyl-coA carboxylase; carboxyltransferase subunit

The structures of the bacterial carboxyltransferase subunit of *Escherichia coli* and *Staphylococcus aureus* acetyl-CoA carboxylase reveal $\alpha_2\beta_2$ heterotetramers whose individual subunits are novel members of the crotonase superfamily. The active site pocket, which is formed by contributions from α and β subunits across a pseudo two-fold dimer interface, is partially sheltered by a zinc-binding domain that is poised to play a

role in shielding the acetyl-CoA substrate during catalysis. The invariant positions of the zinc-binding cysteines within an independent domain in prokaryotic (but not eukaryotic) CT and the inter-specific variation in bacteria that exists within the primary sequence surrounding the zinc site are key features of the enzyme. It follows from these observations that the availability of structures for the CT component of ACC from the two major classes (gram-positive and gram-negative) of pathogenic bacteria has potential to facilitate structure-based design of antimicrobials that possess selective bacterial toxicity and circumvent inhibition of the mammalian enzyme.

REFERENCES

Agar, J., L. Zheng, V. Cash, D. Dean and M. Johnson (2000). "Role of the IscU protein in iron-sulfur cluster biosynthesis: IscS-mediated assembly of a [Fe2S2] cluster in IscU." Journal of the American Chemical Society **122**: 2136-2137.

Agar, J. N., C. Krebs, J. Frazzon, B. H. Huynh, D. R. Dean and M. K. Johnson (2000). "IscU as a scaffold for iron-sulfur cluster biosynthesis: sequential assembly of [2Fe-2S] and [4Fe-4S] clusters in IscU." Biochemistry **39**: 7856-62.

Banerjee, A., E. Dubnau, A. Quemard, V. Balasubramanian, K. S. Um, T. Wilson, D. Collins, G. de Lisle and W. R. Jacobs, Jr. (1994). "inhA, a gene encoding a target for isoniazid and ethionamide in Mycobacterium tuberculosis." Science **263**: 227-30.

Barber, M. C., N. T. Price and M. T. Travers (2005). "Structure and regulation of acetyl-CoA carboxylase genes of metazoa." Biochim Biophys Acta **1733**: 1-28.

Beh, M. G. Strauss, R. Huber, K., Stetter and G. Fuchs (1993). "Enzymes of the reductive citric-acid cycle in the autotrophic eubacterium aquifex-pyrophilus and in the archaebacterium thermoproteu-neutrophilus." Archives of Microbiology **160**: 306-311.

Beinert, H. (2000). "Iron-sulfur proteins: ancient structures, still full of surprises." J Biol Inorg Chem **5**: 2-15.

Beinert, H., R. H. Holm and E. Munck (1997). "Iron-sulfur clusters: nature's modular, multipurpose structures." Science **277**: 653-9.

Beinert, H. and P. Kiley (1996). "Redox control of gene expression involving iron-sulfur proteins. Change of oxidation-state or assembly/disassembly of Fe-S clusters?" FEBS Lett **382**: 218-9; discussion 220-1.

Bertini, I., J. A. Cowan, C. Del Bianco, C. Luchinat and S. S. Mansy (2003). "Thermotoga maritima IscU. Structural characterization and dynamics of a new class of metallochaperone." J Mol Biol **331**: 907-24.

Blanchard, C. Z. and G. L. Waldrop (1998). "Overexpression and kinetic characterization of the carboxyltransferase component of acetyl-CoA carboxylase." J Biol Chem **273**: 19140-5.

Bognar, A. L., C. Osborne and B. Shane (1987). "Primary structure of the Escherichia coli folC gene and its folylpolyglutamate synthetase-dihydrofolate synthetase

product and regulation of expression by an upstream gene." J Biol Chem **262**: 12337-43.

Brunger, A. T., P. D. Adams, G. M. Clore, W. L. DeLano, P. Gros, R. W. Grosse-Kunstleve, J. S. Jiang, J. Kuszewski, M. Nilges, N. S. Pannu, R. J. Read, L. M. Rice, T. Simonson and G. L. Warren (1998). "Crystallography & NMR system: A new software suite for macromolecular structure determination." Acta Crystallogr D Biol Crystallogr **54 (Pt 5)**: 905-21.

Burton, J. D., J. W. Gronwald, D. A. Somers, J. A. Connelly, B. G. Gengenbach and D. L. Wyse (1987). "Inhibition of plant acetyl-coenzyme A carboxylase by the herbicides sethoxydim and haloxyfop." Biochem Biophys Res Commun **148**: 1039-44.

Cairo, G., S. Recalcati, A. Pietrangelo and G. Minotti (2002). "The iron regulatory proteins: targets and modulators of free radical reactions and oxidative damage." Free Radic Biol Med **32**: 1237-43.

Campbell, J. W. and J. E. Cronan, Jr. (2001). "Bacterial fatty acid biosynthesis: targets for antibacterial drug discovery." Annu Rev Microbiol **55**: 305-32.

Cody, G. (2004). "Transition metal sulfides and the origins of metabolism." Annual Review of Earth and Planetary Sciences **32**: 569-599.

Cody, G. D., N. Z. Boctor, T. R. Filley, R. M. Hazen, J. H. Scott, A. Sharma and H. S. Yoder, Jr. (2000). "Primordial carbonylated iron-sulfur compounds and the synthesis of pyruvate." Science **289**: 1337-40.

Collaborative Computational Project, Number 4 (1994). "The CCP4 suite: programs for protein crystallography." Acta Crystallogr D Biol Crystallogr **50**: 760-3.

Crepin, T., E. Schmitt, S. Blanquet and Y. Mechulam (2004). "Three-dimensional structure of methionyl-tRNA synthetase from Pyrococcus abyssi." Biochemistry **43**: 2635-44.

Cronan, J. E., Jr. and G. L. Waldrop (2002). "Multi-subunit acetyl-CoA carboxylases." Prog Lipid Res **41**: 407-35.

D'Agnolo, G., I. S. Rosenfeld, J. Awaya, S. Omura and P. R. Vagelos (1973). "Inhibition of fatty acid synthesis by the antibiotic cerulenin. Specific inactivation of beta-ketoacyl-acyl carrier protein synthetase." Biochim Biophys Acta **326**: 155-6.

Davis, B. K. (2002). "Molecular evolution before the origin of species." Prog Biophys Mol Biol **79**: 77-133.

Davis, M. S., J. Solbiati and J. E. Cronan, Jr. (2000). "Overproduction of acetyl-CoA carboxylase activity increases the rate of fatty acid biosynthesis in Escherichia coli." J Biol Chem **275**: 28593-8.

Diacovich, L., D. L. Mitchell, H. Pham, G. Gago, M. M. Melgar, C. Khosla, H. Gramajo and S. C. Tsai (2004). "Crystal structure of the beta-subunit of acyl-CoA carboxylase: structure-based engineering of substrate specificity." Biochemistry **43**: 14027-36.

Ding, H. and R. J. Clark (2004). "Characterization of iron binding in IscA, an ancient iron-sulphur cluster assembly protein." Biochem J **379**: 433-40.

Ding, H., R. J. Clark and B. Ding (2004). "IscA mediates iron delivery for assembly of iron-sulfur clusters in IscU under the limited accessible free iron conditions." J Biol Chem **279**: 37499-504.

Eck, R. V. and M. O. Dayhoff (1966). "Evolution of the Structure of Ferredoxin Based on Living Relics of Primitive Amino Acid Sequences." Science **152**: 363-366.

Freiberg, C., N. A. Brunner, G. Schiffer, T. Lampe, J. Pohlmann, M. Brands, M. Raabe, D. Habich and K. Ziegelbauer (2004). "Identification and characterization of the first class of potent bacterial acetyl-CoA carboxylase inhibitors with antibacterial activity." J Biol Chem **279**: 26066-73.

Gerlt, J. A. and P. C. Babbitt (2001). "Divergent evolution of enzymatic function: mechanistically diverse superfamilies and functionally distinct suprafamilies." Annu Rev Biochem **70**: 209-46.

Glasfeld, E. and P. Schimmel (1997). "Zinc-dependent tRNA binding by a peptide element within a tRNA synthetase." Biochemistry **36**: 6739-44.

Guchhait, R. B., S. E. Polakis, P. Dimroth, E. Stoll, J. Moss and M. D. Lane (1974). "Acetyl coenzyme A carboxylase system of Escherichia coli. Purification and properties of the biotin carboxylase, carboxyltransferase, and carboxyl carrier protein components." J Biol Chem **249**: 6633-45.

Ha, J. and K. H. Kim (1994). "Inhibition of fatty acid synthesis by expression of an acetyl-CoA carboxylase-specific ribozyme gene." Proc Natl Acad Sci U S A **91**: 9951-5.

Hall, P. R., Y. F. Wang, R. E. Rivera-Hainaj, X. Zheng, M. Pustai-Carey, P. R. Carey and V. C. Yee (2003). "Transcarboxylase 12S crystal structure: hexamer assembly and substrate binding to a multienzyme core." Embo J **22**: 2334-47.

Hayashi, T., O. Yamamoto, H. Sasaki, A. Kawaguchi and H. Okazaki (1983). "Mechanism of action of the antibiotic thiolactomycin inhibition of fatty acid synthesis of Escherichia coli." Biochem Biophys Res Commun **115**: 1108-13.

Heath, R. J., Y. T. Yu, M. A. Shapiro, E. Olson and C. O. Rock (1998). "Broad spectrum antimicrobial biocides target the FabI component of fatty acid synthesis." J Biol Chem **273**: 30316-20.

Heinen, W. and A. M. Lauwers (1996). "Organic sulfur compounds resulting from the interaction of iron sulfide, hydrogen sulfide and carbon dioxide in an anaerobic aqueous environment." Orig Life Evol Biosph **26**: 131-50.

Huber, C., W. Eisenreich, S. Hecht and G. Wachtershauser (2003). "A possible primordial peptide cycle." Science **301**: 938-40.

Huber, C. and G. Wachtershauser (1997). "Activated acetic acid by carbon fixation on (Fe,Ni)S under primordial conditions." Science **276**: 245-7.

Huber, C. and G. Wachtershauser (1998). "Peptides by activation of amino acids with CO on (Ni,Fe)S surfaces: implications for the origin of life." Science **281**: 670-2.

Hugler, M., C. O. Wirsen, G. Fuchs, C. D. Taylor and S. M. Sievert (2005). "Evidence for autotrophic CO2 fixation via the reductive tricarboxylic acid cycle by members of the epsilon subdivision of proteobacteria." J Bacteriol **187**: 3020-7.

James, E. S. and J. E. Cronan (2004). "Expression of two Escherichia coli acetyl-CoA carboxylase subunits is autoregulated." J Biol Chem **279**: 2520-7.

Jensen, L. T. and V. C. Culotta (2000). "Role of Saccharomyces cerevisiae ISA1 and ISA2 in iron homeostasis." Mol Cell Biol **20**: 3918-27.

Jitrapakdee, S. and J. C. Wallace (2003). "The biotin enzyme family: conserved structural motifs and domain rearrangements." Curr Protein Pept Sci **4**: 217-29.

Johnson, D. C., D. R. Dean, A. D. Smith and M. K. Johnson (2005). "Structure, function, and formation of biological iron-sulfur clusters." Annu Rev Biochem **74**: 247-81.

Jones, T. A., J. Y. Zou, S. W. Cowan and Kjeldgaard (1991). "Improved methods for building protein models in electron density maps and the location of errors in these models." Acta Crystallogr A **47 (Pt 2)**: 110-9.

Kato, S., H. Mihara, T. Kurihara, Y. Takahashi, U. Tokumoto, T. Yoshimura and N. Esaki (2002). "Cys-328 of IscS and Cys-63 of IscU are the sites of disulfide bridge formation in a covalently bound IscS/IscU complex: implications for the mechanism of iron-sulfur cluster assembly." Proc Natl Acad Sci U S A **99**: 5948-52.

Kaut, A., H. Lange, K. Diekert, G. Kispal and R. Lill (2000). "Isa1p is a component of the mitochondrial machinery for maturation of cellular iron-sulfur proteins and requires conserved cysteine residues for function." J Biol Chem **275**: 15955-61.

Ke, J., T. N. Wen, B. J. Nikolau and E. S. Wurtele (2000). "Coordinate regulation of the nuclear and plastidic genes coding for the subunits of the heteromeric acetyl-coenzyme A carboxylase." Plant Physiol **122**: 1057-71.

Kent, T. A., J. L. Dreyer, M. C. Kennedy, B. H. Huynh, M. H. Emptage, H. Beinert and E. Munck (1982). "Mossbauer studies of beef heart aconitase: evidence for facile interconversions of iron-sulfur clusters." Proc Natl Acad Sci U S A **79**: 1096-100.

Kent, T. A., M. H. Emptage, H. Merkle, M. C. Kennedy, H. Beinert and E. Munck (1985). "Mossbauer studies of aconitase. Substrate and inhibitor binding, reaction intermediates, and hyperfine interactions of reduced 3Fe and 4Fe clusters." J Biol Chem **260**: 6871-81.

Kerscher, L. and D. Oesterhelt (1981). "The catalytic mechanism of 2-oxoacid:ferredoxin oxidoreductases from Halobacterium halobium. One-electron transfer at two distinct steps of the catalytic cycle." Eur J Biochem **116**: 595-600.

Khoroshilova, N., C. Popescu, E. Munck, H. Beinert and P. J. Kiley (1997). "Iron-sulfur cluster disassembly in the FNR protein of Escherichia coli by O2: [4Fe-4S] to [2Fe-2S] conversion with loss of biological activity." Proc Natl Acad Sci U S A **94**: 6087-92.

Kleywegt, G. J. and T. A. Jones (1996). "xdlMAPMAN and xdlDATAMAN - programs for reformatting, analysis and manipulation of biomacromolecular electron-density maps and reflection data sets." Acta Crystallogr D Biol Crystallogr **52**: 826-8.

Kozaki, A., K. Mayumi and Y. Sasaki (2001). "Thiol-disulfide exchange between nuclear-encoded and chloroplast-encoded subunits of pea acetyl-CoA carboxylase." J Biol Chem **276**: 39919-25.

Krebs, C., J. N. Agar, A. D. Smith, J. Frazzon, D. R. Dean, B. H. Huynh and M. K. Johnson (2001). "IscA, an alternate scaffold for Fe-S cluster biosynthesis." Biochemistry **40**: 14069-80.

Krishna, S. S., I. Majumdar and N. V. Grishin (2003). "Structural classification of zinc fingers: survey and summary." Nucleic Acids Res **31**: 532-50.

Lange, H., A. Kaut, G. Kispal and R. Lill (2000). "A mitochondrial ferredoxin is essential for biogenesis of cellular iron-sulfur proteins." Proc Natl Acad Sci U S A **97**: 1050-5.

Laskowski, R. A., M. W. MacArthur, D. S. Moss and J. M. Thornton (1993). "PROCHECK: a program to check the stereochemical quality of protein structures." J Appl Cryst **26**: 283-291.

Lauble, H., M. C. Kennedy, H. Beinert and C. D. Stout (1992). "Crystal structures of aconitase with isocitrate and nitroisocitrate bound." Biochemistry **31**: 2735-48.

Levert, K. L. and G. L. Waldrop (2002). "A bisubstrate analog inhibitor of the carboxyltransferase component of acetyl-CoA carboxylase." Biochem Biophys Res Commun **291**: 1213-7.

Li, S. J. and J. E. Cronan, Jr. (1992). "The gene encoding the biotin carboxylase subunit of Escherichia coli acetyl-CoA carboxylase." J Biol Chem **267**: 855-63.

Li, S. J. and J. E. Cronan, Jr. (1992). "The genes encoding the two carboxyltransferase subunits of Escherichia coli acetyl-CoA carboxylase." J Biol Chem **267**: 16841-7.

Li, S. J. and J. E. Cronan, Jr. (1993). "Growth rate regulation of Escherichia coli acetyl coenzyme A carboxylase, which catalyzes the first committed step of lipid biosynthesis." J Bacteriol **175**: 332-40.

Li, S. J., C. O. Rock and J. E. Cronan, Jr. (1992). "The dedB (usg) open reading frame of Escherichia coli encodes a subunit of acetyl-coenzyme A carboxylase." J Bacteriol **174**: 5755-7.

Mansy, S. S., G. Wu, K. K. Surerus and J. A. Cowan (2002). "Iron-sulfur cluster biosynthesis. Thermatoga maritima IscU is a structured iron-sulfur cluster assembly protein." J Biol Chem **277**: 21397-404.

Marrakchi, H., Y. M. Zhang and C. O. Rock (2002). "Mechanistic diversity and regulation of Type II fatty acid synthesis." Biochem Soc Trans **30**: 1050-5.

Martin, W. and M. J. Russell (2003). "On the origins of cells: a hypothesis for the evolutionary transitions from abiotic geochemistry to chemoautotrophic prokaryotes, and from prokaryotes to nucleated cells." Philos Trans R Soc Lond B Biol Sci **358**: 59-83; discussion 83-5.

Martin, W., B. Stoebe, V. Goremykin, S. Hapsmann, M. Hasegawa and K. V. Kowallik (1998). "Gene transfer to the nucleus and the evolution of chloroplasts." Nature **393**: 162-5.

Menichetti, F. (2005). "Current and emerging serious Gram-positive infections." Clin Microbiol Infect **11 Suppl 3**: 22-8.

Milner-White, E. J., J. W. Nissink, F. H. Allen and W. J. Duddy (2004). "Recurring main-chain anion-binding motifs in short polypeptides: nests." Acta Crystallogr D Biol Crystallogr **60**: 1935-42.

Milner-White, E. J. and M. J. Russell (2005). "Sites for phosphates and iron-sulfur thiolates in the first membranes: 3 to 6 residue anion-binding motifs (nests)." Orig Life Evol Biosph **35**: 19-27.

Moura, J. J., I. Moura, T. A. Kent, J. D. Lipscomb, B. H. Huynh, J. LeGall, A. V. Xavier and E. Munck (1982). "Interconversions of [3Fe-3S] and [4Fe-4S] clusters. Mossbauer and electron paramagnetic resonance studies of Desulfovibrio gigas ferredoxin II." J Biol Chem **257**: 6259-67.

Muhlenhoff, U., N. Richhardt, J. Gerber and R. Lill (2002). "Characterization of iron-sulfur protein assembly in isolated mitochondria. A requirement for ATP, NADH, and reduced iron." J Biol Chem **277**: 29810-6.

Murshudov, G. N., A. A. Vagin and E. J. Dodson (1997). "Refinement of macromolecular structures by the maximum-likelihood method." Acta Crystallogr D Biol Crystallogr **53**: 240-55.

Murzin, A. G. (1998). "How far divergent evolution goes in proteins." Curr Opin Struct Biol **8**: 380-7.

Nakajima, T., Y. Yabushita and I. Tabushi (1975). "Amino acid synthesis through biogenetic-type CO2 fixation." Nature **256**: 60-1.

National Noscomial Infections Surveillance (2004) "National Nosocomial Infections Surveillance (NNIS) System Report, data summary from January 1992 through June 2004, issued October 2004." Am J Infect Control **32**: 470-85.

Ollagnier-de-Choudens, S., T. Mattioli, Y. Takahashi and M. Fontecave (2001). "Iron-sulfur cluster assembly: characterization of IscA and evidence for a specific and functional complex with ferredoxin." J Biol Chem **276**: 22604-7.

Otwinowski, Z. and W. Minor (1997). "Processing of X-ray diffraction data collected in oscillation mode." Macromolecular crystallography, pt A **276**: 307-326.

Page, R. A., S. Okada and J. L. Harwood (1994). "Acetyl-CoA carboxylase exerts strong flux control over lipid synthesis in plants." Biochim Biophys Acta **1210**: 369-72.

Perrakis, A., M. Harkiolaki, K. S. Wilson and V. S. Lamzin (2001). "ARP/wARP and molecular replacement." Acta Crystallogr D Biol Crystallogr **57**: 1445-50.

Plank, D. W., M. C. Kennedy, H. Beinert and J. B. Howard (1989). "Cysteine labeling studies of beef heart aconitase containing a 4Fe, a cubane 3Fe, or a linear 3Fe cluster." J Biol Chem **264**: 20385-93.

Pohlmann, J., T. Lampe, M. Shimada, P. G. Nell, J. Pernerstorfer, N. Svenstrup, N. A. Brunner, G. Schiffer and C. Freiberg (2005). "Pyrrolidinedione derivatives as antibacterial agents with a novel mode of action." Bioorg Med Chem Lett **15**: 1189-92.

Powers, J. H. (2004). "Antimicrobial drug development--the past, the present, and the future." Clin Microbiol Infect **10 Suppl 4**: 23-31.

Rees, D. C. (2002). "Great metalloclusters in enzymology." Annu Rev Biochem **71**: 221-46.

Russell, M. J. and A. J. Hall (1997). "The emergence of life from iron monosulphide bubbles at a submarine hydrothermal redox and pH front." J Geol Soc London **154**: 377-402.

Sasaki, Y., Y. Nagano, S. Morioka, H. Ishikawa and R. Matsuno (1989). "A chloroplast gene encoding a protein with one zinc finger." Nucleic Acids Res **17**: 6217-27.

Schilke, B., C. Voisine, H. Beinert and E. Craig (1999). "Evidence for a conserved system for iron metabolism in the mitochondria of Saccharomyces cerevisiae." Proc Natl Acad Sci U S A **96**: 10206-11.

Schwartz, C. J., O. Djaman, J. A. Imlay and P. J. Kiley (2000). "The cysteine desulfurase, IscS, has a major role in in vivo Fe-S cluster formation in Escherichia coli." Proc Natl Acad Sci U S A **97**: 9009-14.

Serre, L., G. Verdon, T. Choinowski, N. Hervouet, J. L. Risler and C. Zelwer (2001). "How methionyl-tRNA synthetase creates its amino acid recognition pocket upon L-methionine binding." J Mol Biol **306**: 863-76.

Shah, P. M. (2005). "The need for new therapeutic agents: what is the pipeline?" Clin Microbiol Infect **11 Suppl 3**: 36-42.

Sherman, J. M., E. M. Stone, L. L. Freeman-Cook, C. B. Brachmann, J. D. Boeke and L. Pillus (1999). "The conserved core of a human SIR2 homologue functions in yeast silencing." Mol Biol Cell **10**: 3045-59.

Spellberg, B., J. H. Powers, E. P. Brass, L. G. Miller and J. E. Edwards, Jr. (2004). "Trends in antimicrobial drug development: implications for the future." Clin Infect Dis **38**: 1279-86.

Stephens, P. J., D. R. Jollie and A. Warshel (1996). "Protein Control of Redox Potentials of Ironminus signSulfur Proteins." Chem Rev **96**: 2491-2514.

Strain, J., C. R. Lorenz, J. Bode, S. Garland, G. A. Smolen, D. T. Ta, L. E. Vickery and V. C. Culotta (1998). "Suppressors of superoxide dismutase (SOD1) deficiency in Saccharomyces cerevisiae. Identification of proteins predicted to mediate iron-sulfur cluster assembly." J Biol Chem **273**: 31138-44.

Takahashi, Y. and M. Nakamura (1999). "Functional assignment of the ORF2-iscS-iscU-iscA-hscB-hscA-fdx-ORF3 gene cluster involved in the assembly of Fe-S clusters in Escherichia coli." J Biochem (Tokyo) **126**: 917-26.

Tokumoto, U., S. Nomura, Y. Minami, H. Mihara, S. Kato, T. Kurihara, N. Esaki, H. Kanazawa, H. Matsubara and Y. Takahashi (2002). "Network of protein-protein interactions among iron-sulfur cluster assembly proteins in Escherichia coli." J Biochem (Tokyo) **131**: 713-9.

Tokumoto, U. and Y. Takahashi (2001). "Genetic analysis of the isc operon in Escherichia coli involved in the biogenesis of cellular iron-sulfur proteins." J Biochem (Tokyo) **130**: 63-71.

Wachtershauser, G. (1988). "Before enzymes and templates: theory of surface metabolism." Microbiol Rev **52**: 452-84.

Wachtershauser, G. (1990). "Evolution of the first metabolic cycles." Proc Natl Acad Sci U S A **87**: 200-4.

Wachtershauser, G. (1992). "Groundworks for an evolutionary biochemistry: the iron-sulphur world." Prog Biophys Mol Biol **58**: 85-201.

Watson, J. D. and E. J. Milner-White (2002). "A novel main-chain anion-binding site in proteins: the nest. A particular combination of phi,psi values in successive residues gives rise to anion-binding sites that occur commonly and are found often at functionally important regions." J Mol Biol **315**: 171-82.

Wollenberg, M., C. Berndt, E. Bill, J. D. Schwenn and A. Seidler (2003). "A dimer of the FeS cluster biosynthesis protein IscA from cyanobacteria binds a [2Fe2S] cluster between two protomers and transfers it to [2Fe2S] and [4Fe4S] apo proteins." Eur J Biochem **270**: 1662-71.

Wu, G., S. S. Mansy, C. Hemann, R. Hille, K. K. Surerus and J. A. Cowan (2002). "Iron-sulfur cluster biosynthesis: characterization of Schizosaccharomyces pombe Isa1." J Biol Inorg Chem **7**: 526-32.

Wu, G., S. S. Mansy, S. P. Wu Sp, K. K. Surerus, M. W. Foster and J. A. Cowan (2002). "Characterization of an iron-sulfur cluster assembly protein (ISU1) from Schizosaccharomyces pombe." Biochemistry **41**: 5024-32.

Wu, S. P. and J. A. Cowan (2003). "Iron-sulfur cluster biosynthesis. A comparative kinetic analysis of native and Cys-substituted ISA-mediated [2Fe-2S]2+ cluster transfer to an apoferredoxin target." Biochemistry **42**: 5784-91.

Wu, S. P., G. Wu, K. K. Surerus and J. A. Cowan (2002). "Iron-sulfur cluster biosynthesis. Kinetic analysis of [2Fe-2S] cluster transfer from holo ISU to apo Fd: role of redox chemistry and a conserved aspartate." Biochemistry **41**: 8876-85.

Yoon, T. and J. A. Cowan (2003). "Iron-sulfur cluster biosynthesis. Characterization of frataxin as an iron donor for assembly of [2Fe-2S] clusters in ISU-type proteins." J Am Chem Soc **125**: 6078-84.

Zhang, H., Z. Yang, Y. Shen and L. Tong (2003). "Crystal structure of the carboxyltransferase domain of acetyl-coenzyme A carboxylase." Science **299**: 2064-7.

Zheng, L., M. C. Kennedy, G. A. Blondin, H. Beinert and H. Zalkin (1992). "Binding of cytosolic aconitase to the iron responsive element of porcine mitochondrial aconitase mRNA." Arch Biochem Biophys **299**: 356-60.